POLITECNICO DI TORINO

Master Degree in Mechatronic Engineering

Department of Control and Computer Engineering

Modeling and experimental validation of the implement-chassis interaction for construction machines

Candidate:

Daniele Colombara

Advisor:

Prof. Luigi Mazza

External advisors:

Prof. Andrea Vacca

Dott. Addison Alexander

10/12/2018

Abstract

Wheel loaders are everyday off-road machines heavily used worldwide for several different reasons.

This thesis aims in the development of both a numerical and an analytical model for the digging system of a generic wheel loader. Knowing the geometric configuration (boom and bucket angles or lift and tilt cylinders extensions) at each instant, both the models are able to compute the location, in a two-dimensional plane, of a set of points belonging to the system. These points are then used to calculate the forces required at the hydraulic cylinders to balance the external forces which can be either, in the simplest case, just the component weights, or the forces exchanged at the bucket during a normal loading cycle. The models are subsequently validated through a comparison between experimental field test data and data generated through the simulated models.

Finally, the aforementioned models serve for computing external forces acting on the bucket. The models will start from the geometric configuration (boom and bucket angles sensed from the reference machine) and the tilting and lifting cylinder pressures (sensed from the cylinder rods and pistons) to compute the forces along x and z axes acting at the bucket center of gravity. This represents the inverse procedure with respect to the one that computes the cylinder pressures starting from the geometric configuration. Thus, in addition, with this work it would be possible to estimate how the forces exchanged at the bucket are reflected into the vehicle dynamics since these models compute the reactions forces acting at every hinge of the implement, including the chassis-implement connection.

In conclusion, the models developed will not be just useful for having a general idea of the excavation system behavior by itself, but might as well be used for improving other currently ongoing investigations, such as: developing better traction control models, vehicle dynamic models, active oscillations damping, etc.

As part of a further work, a concept for a work pile model able to express all the forces exchanged between bucket and pile itself during digging operations is investigated here. Thus, as future work it is here proposed trying to validate, through the utilization of the digging force models, this new concept of pile model that focuses on the pile-bucket interaction forces.

Contents

List of Figures

Chapter 1

Introduction

The development of well-designed vehicle systems always maintains in tension three distinct goals: productivity, safety, and cost. Often these objectives tend to work against each other, with solutions that improve one factor negatively impacting the other two. However, innovation in vehicle systems occurs when systems are developed which can simultaneously benefit all three of these metrics. Recently, academic and industry research groups in other fields have begun investigating the feasibility of incorporating geometric and dynamic force models into their existing systems. This is particularly true of off-road vehicles such as construction equipment machineries (Fig. 1.1), where safety, productivity, and cost are emphasized to a heightened degree, due to the breakneck pace and the immense loads and forces which are involved in their day-to-day operations in many industries.

1.1   Problem Definition

Off-road machineries are subjected to several studies in order to generally increase productivity, safety and reduce cost. The field in which on-going researches are aiming is wide due to the high working principle difference of these machines. For the purpose of this work, a narrow analysis to wheel loader vehicles is performed. The research team was donated a wheel loader with two main research purposes:

1. Develop an electro-hydraulic traction control system. Due to the usually heavy ground conditions and critical working operations of these machines, wheel loaders are one of the main off-road vehicle types with traction control on-going researches. The system basically prevents the tires wear decreasing costs also for the gas needed

and increases the machine efficiency (no or less tire slip leads to faster manoeuvres and easier working operations).

FIGURE 1.1: Examples of off-road heavy duty machines

2. Develop an active ride control. Due to the mechanical configuration of a wheel loader, being it not equipped with a suspension system, several and critical vibrations are characteristic working conditions, especially after the completion of a digging cycle when moving the dirt in the bucket from one part of the site to another one. Without going into much details, an active ride control system tries to decrease the oscillations magnitude by playing with the hydraulic actuators pressures.

The chassis-implement interaction model was developed for improving these two on-going researches and to simplify their work as follows:

- TC system $\longrightarrow$ in the previously developed model of the traction control system, the pile was modelled simply as a spring-damper parallel connection fixed at a certain high. Therefore, it is clear how, for example, all the vertical forces acting on the bucket were not considered. Hence, with a chassis-implement interaction model, a clearer trend of the exchanged forces could be achieved and, consequently, could improve the overall performance of the traction control system. Moreover, while developing the TC system, only the boom position was computable and necessary. Now, by also knowing the bucket position for each configuration, several other computations can be performed as, for example, measuring highs, computing

power required by the tilting actuator at each digging cycle, optimize the scooping procedure by finding the best bucket-pile trajectory, etc.

- AR control system $\longrightarrow$ in the currently used and under study active ride control system, the main goal is trying to isolate the implement from the rest of the machine in order to not propagate oscillations coming from the payload on the bucket. By increasing or decreasing the lifting cylinder pressures, it is possible to reduce the oscillations seen at the boom-chassis and lifting cylinders-chassis attachments. Therefore, since the chassis-implement interaction model computes also reaction forces at every hinge in the vehicle, it is clear how my work could be useful and powerful for an improvement of the aforementioned active ride control system. By controlling the meter in (flow going from the pump into the actuator piston side) and the meter out (flow going from the actuator rod side to tank) based on pressure or acceleration feedbacks, the system is able to cut or at least minimize the oscillations seen at the operating cabin.

Hence, it is clear here how a model expressing the geometry configuration (a set of point location) and the inter-exchanged forces inside the implement could be useful for these two on-going researches. It is important to say that these are just two of the many possible utilization of the model that has been developed. Nevertheless, this was exactly the main reason behind the start of my project. In the following sections an overview in how the models have been developed and validated is explained.

1.2 Research Goals

The goal of this work is to develop and describe a sound methodology for the design of a chassis-implement interaction system for heavy duty off-road machines. In order to achieve this, the following objectives were defined:

- Determine the behaviour of bucket-pile exchanged forces, with the purpose of understanding the interaction forces magnitude.

- Develop and simulate an analytical model able to represent pre-defined points of the system in space as function of either the hydraulic actuators displacements or the boom and bucket angle. Furthermore, reaction forces at those points are added in order to have an overview of the whole system dynamics.

- Develop and simulate a numerical model able to validate the analytical model ascertaining the its geometric properties and dynamic ones (actuating forces).

- Design and perform experiments to demonstrate that both the models behave correctly with respect to the reference machine for which they have been developed for.

- Design a work pile model that takes into account all the forces inter-exchanged with the working machinery. This model would substitute an elementary one used for the traction control on-going research.

To this end, one of the original contributions of this work is the creation of a work pile model that takes into account all the forces inter-exchanged with the working machinery. Model parameters are chosen based on excavation and milling data to ensure that the model matches the pile behaviour as closely as possible. The simulation makes it possible to understand the force interactions between the machine and the pile without having to conduct tests for each case. Moreover, an analytical and a numerical model of the chassis-implement interaction are developed in order to understand the vehicle dynamics during steady state and digging operations. Finally, the system was implemented on a real-world machine in order to assess the tangible benefits of having such working models in realistic conditions. The reference machine available to the research team was modified to create a prototype with the installation of the several needed sensors.

1.3   Reference Machine

The machine used as a reference vehicle in this work is a wheel loader. Wheel loaders are large front-loading tractors used primarily for digging and transporting material at work sites. They can also be used for pushing and pulling in applications such as demolition, ground grading, and snow removal. In all of these operating modes, large forces on both the hydraulic actuators and on the implement itself are in play. Because of the prevalence of these machines and their propensity for heavy duty cycles as scooping and transportation, they represent one of the most significant cases for the realization and design of a chassis-implement model. The incorporation of a chassis-implement interaction system will aid the operation of the wheel loader, potentially cutting down costs, while increasing productivity (in terms of controllability). Despite the relatively narrow focus on wheel loaders for this research, the work presented here is applicable to a wide array of off-road systems with similar implement realization (meaning boom and bucket connection through a link and bellcrank). The overall simulation process and controls methods are generally valid for many different machines. A 16-metric ton wheel loader (Fig. 1.2) was donated to the research team for use as the development prototype. It is equipped with

FIGURE 1.2: Wheel loader used as a reference vehicle in this research

a standard configuration boom and bucket as the front implement, which is actuated by a high-pressure hydraulic circuit. Power is transferred from the combustion engine to the wheels through use of a torque converter, a locked transfer case to transmit torque to the driveshaft, and open differentials at each axle.

Chapter 2

Dynamic System Model

Having seen the main reasons behind the necessity of this work, we can now focus on attention on the dynamic system model that has been developed for the traction control research. Without going into much details on every block of all of the various components of the vehicle dynamics model, a diagram showing the connections among the various sub-models (designed for simulating the vehicle dynamics) is shown in Fig. 2.1:
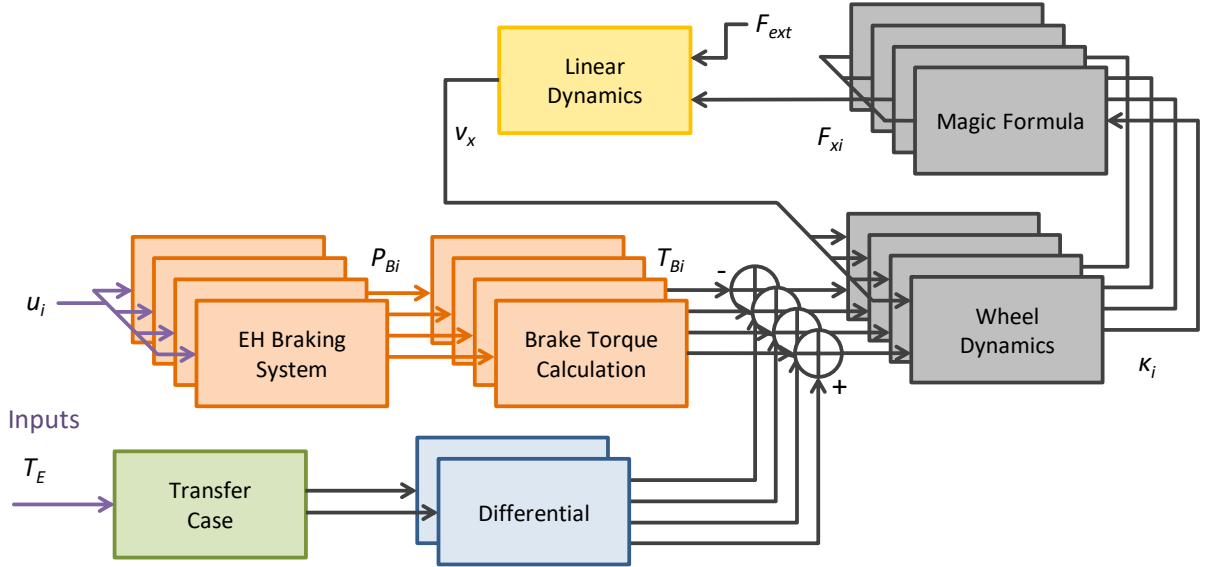
FIGURE 2.1: Block diagram of full vehicle dynamics model

where the primary inputs to the system are the engine torque T_E and the commands to the brakes u_i. The brake commands can come either from the operator pressing the brake pedal or from the TC system utilizing the electro-hydraulic capacity of the modified system. The engine torque is distributed to each of the wheels through the transfer case and differentials, then those distributed torque values are summed with the braking torque.

The resultant torque is used in the equations of motion for the wheels. Using the wheel slip at each wheel κ_i, the longitudinal force F_{xi} is calculated. From that and other forces, the linear motion of the simulated vehicle is updated. All of these various sub-models work together to generate a suitable estimate of the wheel loader behavior under various conditions and inputs. Part of this work therefore aims in modifying and enhancing the Vehicle Dynamics block: by having a more accurate external interaction force estimate on the bucket edge, the system overall behaviur tends to achieve a better simulated dynamics. It is worth saying that this work improves the vehicle overall behaviur just during digging operations (or when there is an inter-exchange of forces between implement and external world). Inside the Vehicle Dynamics sub-model, we can find a Vehicle Velocity sub-sub-model, as shown in Fig. 2.2:
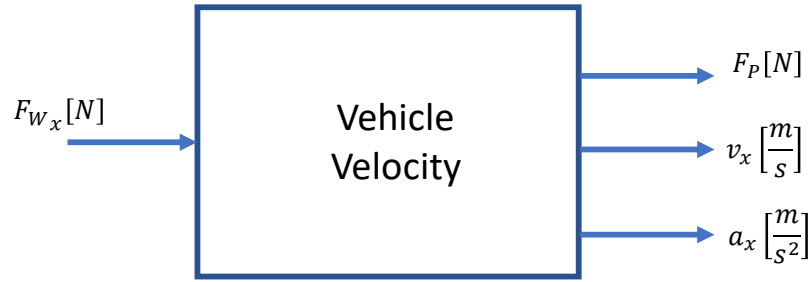
FIGURE 2.2: Sub-system computing the vehicle velocity

where the only input is the longitudinal pushing force of all the four wheels and the outputs are the horizontal acceleration a_x, velocity v_x and the force coming from the pile F_P (or more in general any external force acting on the bucket).

Chapter 3

Analytical Model

The goal of this chapter is to introduce the analytical model developed for the excavation system of a generic wheel loader. Firstly, the geometry computation of the system is investigated. After that, a static force analysis is performed in order to find the force required at the actuators to balance the system. Once the math behind these computations is validated through a comparison with a numerical model and experimental tests, the procedure is inverted in order to find the external forces exchanged at the bucket center of gravity, starting from the system configuration and the cylinder pressures (forces). For the purpose of my research, a 16-tons wheel loader dimensions and data sheets are used. Nevertheless, the model is capable of switching into another wheel loader configuration, keeping its correctness, just by changing a small set of predefined lengths and weights. This decoupling from a very specific machine was one of the main priorities during the model developing phase.

3.1   Methodology

The analytical model expressing the system geometry is developed as follows: the project sponsor furnished a file in which every point location was represented with respect to a fixed point (usually one of the hinges belonging to the implement system) with their respective lengths. This geometric data was given for every hinge composing the system plus the centers of gravity of boom, bellcrank and bucket. Thus, starting from the point locations of each sub-system, boom, bucket and bellcrank, a MATLAB/Excel code is developed. Every relevant point needed for the system (hinge on the implement and centers of gravity) is therefore expressed in a two dimensional plane (x and z axes) with respect to a fixed reference frame called O, being the boom-chassis attachment. So,

in conclusion, the main goal of this model is obtaining a continuous point location as function of the cylinders displacements. All the computations performed on the needed triangles, as we are seeing in the next section, rely just in sine and cosine laws and basic trigonometric rules. After that, in section 3.4, on each hinge reaction forces are included (vertical and an horizontal force o x and z axes, respectively): the main goal becomes computing the needed forces at the hydraulic actuators in order to balance the system. The disturbance, being the external forces acting on the system, can be either just the weight of a sub-systems (boom, bellcrank and bucket) or, in addition to those, any exterior force exchanged at the bucket center of gravity.

3.2   System Definition

The main purpose of the analytical model is having a continuous geometric computation of predetermined point positions as function of the hydraulic cylinder extensions, in order to always have a snapshot of the particular geometric configuration in which the wheel loader excavation system is. The convention chosen for the points representation, that is going to be used from now on to simplify the equations and notations, of any generic wheel loader is expressed in Fig 3.1.
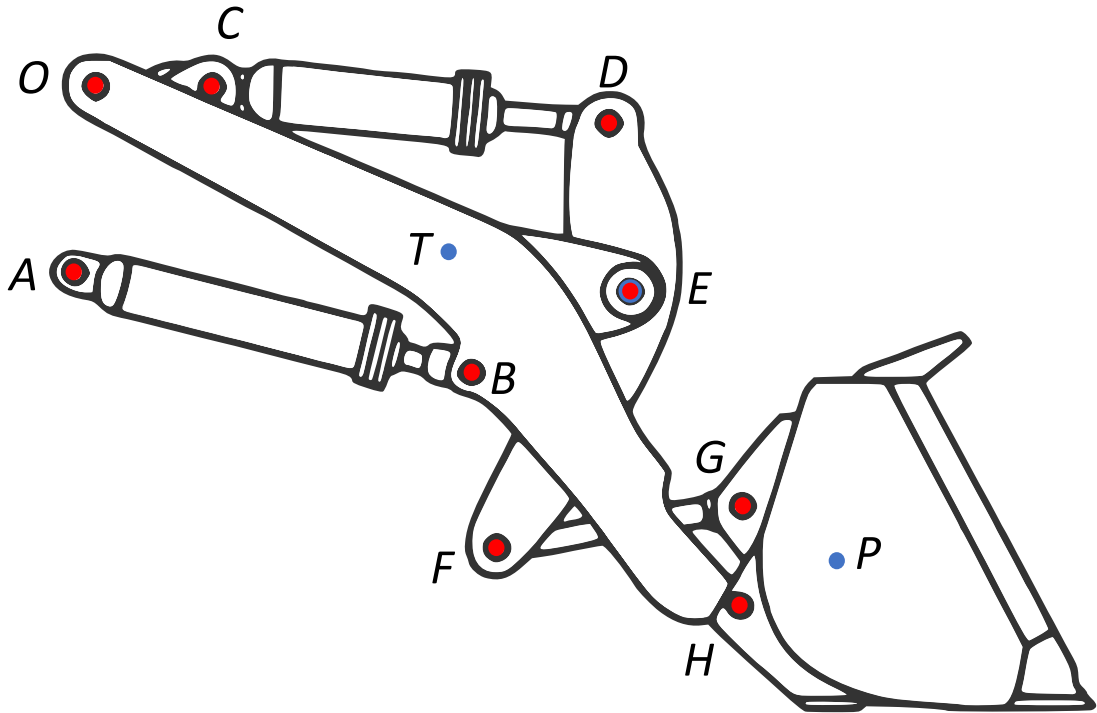

FIGURE 3.1: 2D side view of the excavation system and reference points

Points O, A and C are, respectively, the boom, lifting and tilting cylinders attachments to the chassis. The other points belonging to the boom are B, rod termination of the lifting cylinders, point E, inter exchanged with the bellcrank, and H, bottom hinge for the bucket connection. The bellcrank, being the mechanical structure allowing the bucket tilting, is composed by points D, rod end connection of the tilting cylinder, point E, inter exchanged with the boom, and point F, semi direct connection with the bucket through the $\overline{FG}$ linkage. The remaining point is G, coupled with the tilting system due the link $\overline{FG}$, placed at the revolute joint on the bucket top part, completing the system with the bucket edge. Finally, highlighted in blue, we find points T and P, boom and bucket centers of gravity, respectively. Since the bellcrank CoG lies at a maximum distance of ≈ 2mm along the three axes with respect to point E, for simplification it will be considered exactly in E, due to the negligible lever arm. Besides, the link $\overline{FG}$ weight, being ≈ 82kg, is not taken into account for simplification purposes as we will better see in the force balance section. Therefore, its center of gravity is not represented in Fig. 3.1. Besides, as it is going to be expressed in the next section, a simplification for representing lifting and tilting cylinder extensions is performed, being L_1 and L_2 respectively.

As shown in Fig 3.2, the model computes boom and bucket angles starting form the cylinder displacements. The boom angle is considered as, with respect to horizontal axis x, the angle given by the boom position measured by the OH displacement, since both points O and H lies on the same line.
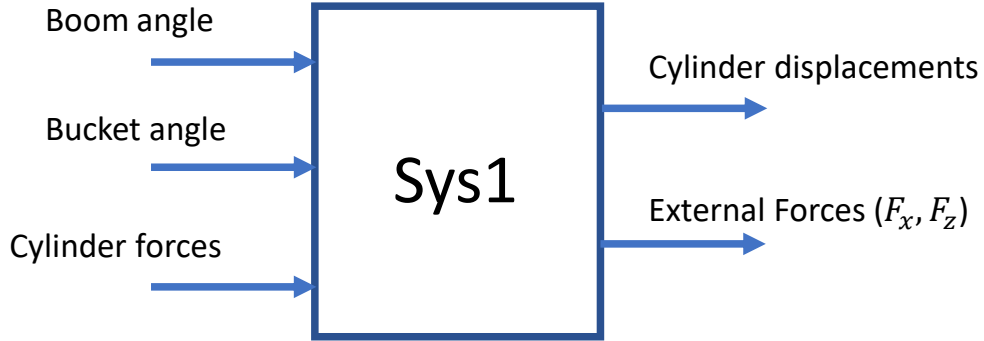

FIGURE 3.2: Overview of the direct kinematic model

$$\theta_{boom} = \begin{cases} \theta_{boom} \geq 0, & \text{if} \quad H_z \geq 0 \\ \theta_{boom} < 0, & \text{if} \quad H_z < 0 \end{cases} \tag{3.1}$$

The boom angle strictly depends on just the chassis-boom distance $\overline{AB}$:

$$\theta_{boom} = f(L_1) \tag{3.2}$$

Similar reasoning is valid for the bucket angle, being, again with respect to the horizontal axis x, the angle given by the bucket plate inclination:

$$\theta_{bkt} = \begin{cases} \theta_{bkt} \geq 0, & \text{if} \quad H_z \geq Edge_z + z_{offset} \\ \theta_{bkt} < 0, & \text{if} \quad H_z < Edge_z + z_{offset} \end{cases} \tag{3.3}$$

where z_{offset} represents the offset angle characteristic of the mechanical design of the bucket, as it is expressed clearly afterwards.

The bucket angle however depends on both lifting and tilting cylinder displacements, therefore is going to be a function depending from two variables, meaning:

$$\theta_{bkt} = f(L_1, L_2) \tag{3.4}$$

Besides angles computation, and therefore every point location of the system, a set of force and moment balances is solved, leading our system to calculate the forces needed on the lifting and tilting cylinders in order to balance the parts composing the implement system weights in that particular configuration (that can be expressed either with the cylinders extensions or with the boom and bucket angles). In the next sections, the method in which the geometry and the hydraulic actuator pressures (thus the actuating forces) computations are calculated is explained.

3.3   Kinematic Analysis

The geometry computation provides, in terms of x and z coordinates, the points location for each cylinder extension dataset. For the purpose of simplifying the convention, from now on, the boom cylinder length $(\overline{AB})$ is referred as L_1 whilst the tilting one $(\overline{CD})$ as L_2. Therefore, the respective extensions are going to be L_{1ex} and L_{2ex}. So, since for our machine we have:

$$0 \leq L_{1ex} \leq 0.828 \text{ m} \tag{3.5}$$

$$0 \leq L_{2ex} \leq 0.6294 \text{ m} \tag{3.6}$$

and therefore, given the closed lengths of both the cylinders, we will have:

$$L_{1closed} = 1.39 \text{ m} \longrightarrow 1.39 \text{ m} \leq L1 \leq 2.218 \text{ m}$$

$$L_{2closed} = 1.1699 \text{ m} \longrightarrow 1.1699 \text{ m} \leq L2 \leq 1.7993 \text{ m}$$

In this section all the points belonging to the implement system shown in Fig. 3.1 are computed and the procedure is explained. Center of gravity locations are going to be computed too. It is worth of mention anyways that they will be used just for section 3.4, where forces are going to be included into the system.

First of all, the computation of the boom angle is required in order to express the position in space of all the points belonging to the boom. In Fig 3.3, recalling the convention defined in 3.1, the logic behind the boom angle computation is shown:
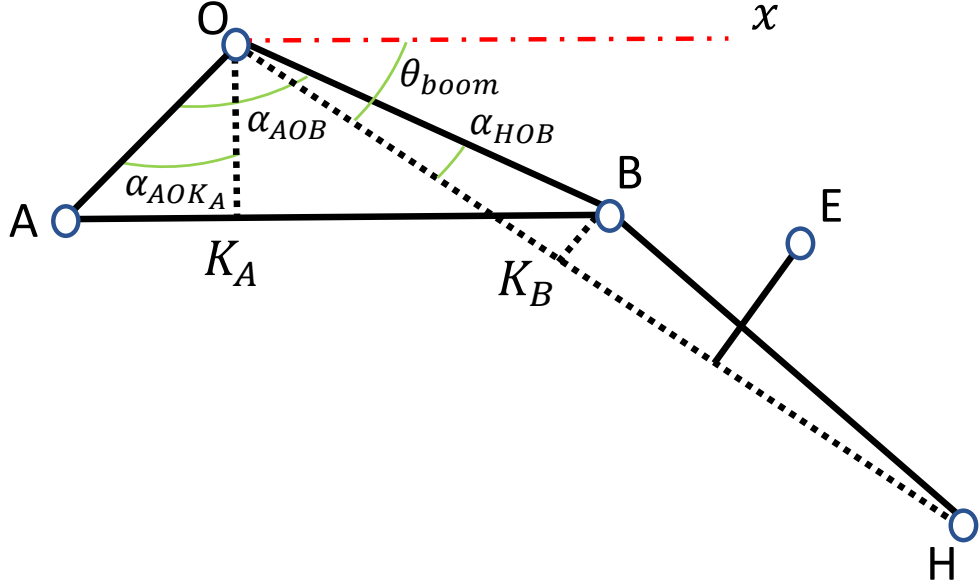
FIGURE 3.3: Triangles solved for the boom angle computation

being:

$$\alpha_{AOB} = \cos^{-1}\left(\frac{\overline{OA}^2 + \overline{OB}^2 - L1^2}{2\overline{OA}\,\overline{OB}}\right) \tag{3.7}$$

$$\alpha_{HOB} = \tan^{-1}\left(\frac{\overline{BK_B}}{\overline{OK_B}}\right) \tag{3.8}$$

$$\alpha_{AOK_A} = \tan^{-1}\left(\frac{\overline{AK_A}}{\overline{OK_A}}\right) \tag{3.9}$$

then, it is clear that the boom angle can be computed as:

$$\theta_{boom} = -\left(\frac{\pi}{2} - (\alpha_{AOB} - \alpha_{AOK_A}) + \alpha_{HOB}\right) \tag{3.10}$$

where the sign before the parenthesis recalls the boom angle sign convention expressed in equation 3.1. It is clear how the boom angle magnitude changes in relation with the lifting cylinder extension $\overline{AB}$. Consequently, all the points belonging to the boom are

computable, respectively in x and z directions, just as product between corresponding lever times cosine and sine of their relative angles as follows:

$$H = [H_x, H_z] = \begin{cases} H_x = \overline{OH} \cos\left(\theta_{boom}\right) \\ H_z = \overline{OH} \sin\left(\theta_{boom}\right) \end{cases} \tag{3.11}$$

since point H is the other reference point for the boom angle computation. For points B and E, since they lay on the boom with a different z with respect to $\overline{OH}$, an offset angle has to be computed and taken into account:

$$B = [B_x, B_z] = \begin{cases} B_x = \overline{OB} \cos\left(\theta_{boom} + \alpha_{HOB}\right) \\ B_z = \overline{OB} \sin\left(\theta_{boom} + \alpha_{HOB}\right) \end{cases} \tag{3.12}$$

where, regarding point B, α_{HOB} barely influences the final result due to its small value. For the last point on the boom E, the offset angle is first shown in Fig 3.4:

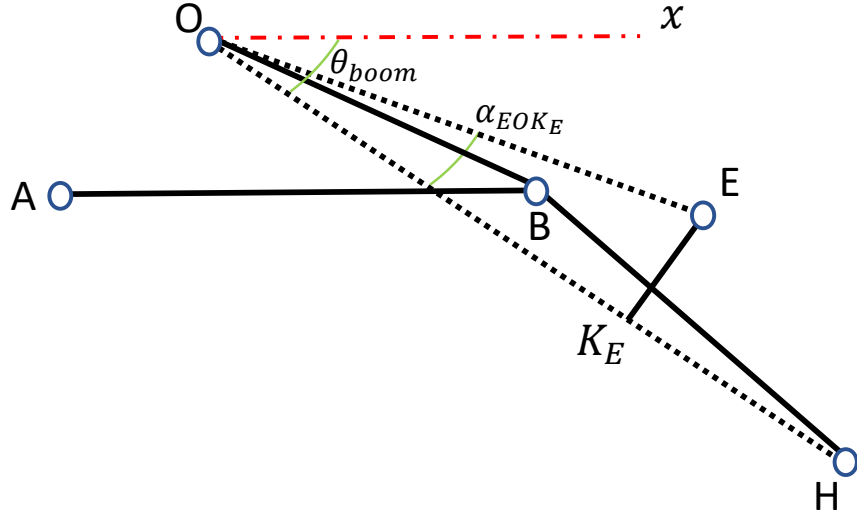FIGURE 3.4: Triangles solved for the point E offset angle computation

where:

$$\alpha_{EOK_E} = \tan^{-1}\left(\frac{\overline{EK_E}}{\overline{OK_E}}\right) \tag{3.13}$$

and hence E location it can be computed as:

$$E = [E_x, E_z] = \begin{cases} E_x = \overline{OE} \cos\left(\theta_{boom} + \alpha_{EOK_E}\right) \\ E_z = \overline{OE} \sin\left(\theta_{boom} + \alpha_{EOK_E}\right) \end{cases} \tag{3.14}$$

We can now step forward to the next subsystem, being the bellcrank. One out of three points belonging to the bellcrank is already known (E). In order to find the remaining two, since the position of C is now known too, it is possible to use again the lever and sine/cosine method but now with respect to the known point E.

First of all, the angle of point D with respect to the fixed tilting cylinder chassis attachment C and the boom connection E has to be found. The Fig 3.5 shows the geometry and triangles needed:
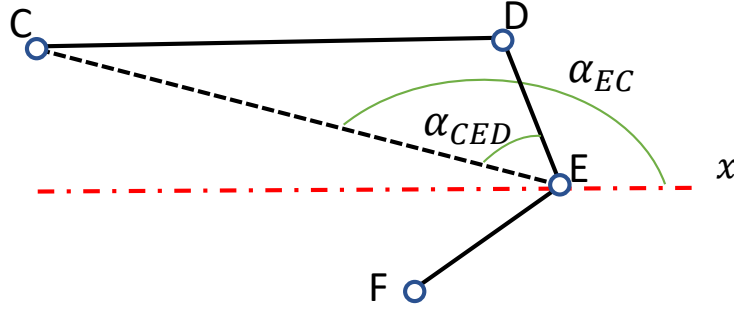
FIGURE 3.5: Triangle solved for the point D computation

thus, by applying the cosine law and remembering that the length $\overline{CD}$ is L_2, we obtain:

$$\alpha_{CED} = \cos^{-1}\left(\frac{\overline{CE}^2 + \overline{ED}^2 - L2^2}{2\,\overline{CE}\,\overline{ED}}\right) \tag{3.15}$$

where the link $\overline{ED}$ is a fixed distance given by the geometry of the bellcrank and where the length $\overline{CE}$, changing in time, can be easily computed through the Pythagoras theorem as:

$$\overline{CE} = \sqrt{(E_z - C_z)^2 + (E_x + C_x)^2}$$

since both E and C are known for every boom configuration.

Hence, since point C is fixed and E known, the angle between these two, keeping point E as fixed reference frame, with respect to the horizontal axis x, can be found as follows:

$$\alpha_{EC_x} = \tan^{-1}\left(\frac{E_z - C_z}{E_x - C_x}\right) \gtrless 0 \quad \text{if} \quad E_z \gtrless C_z \tag{3.16}$$

since, due to mechanical constraints of the system, configurations where $E_x \leq C_x$ are not achievable. Therefore, point D can be easily computed as:

$$D = [D_x, D_z] = \begin{cases} D_x = E_x + \overline{ED}\cos\left(\alpha_{EC_x} - \alpha_{CED}\right) \\ D_z = E_z + \overline{ED}\sin\left(\alpha_{EC_x} - \alpha_{CED}\right) \end{cases} \tag{3.17}$$
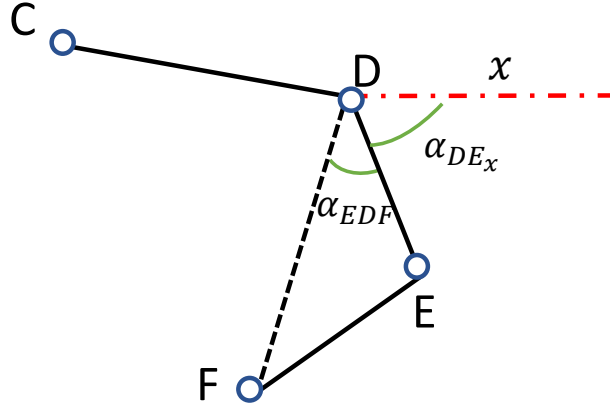
FIGURE 3.6: Angles and triangles for F computation

Since the bellcrank geometry is fixed and not changing in time, the computation of point F location is performed as follows: the angle between D and E, being it α_{DE_x}, is computed through simply an atan2 function; then, since the bellcrank triangle is independent, we know from factory data the α_{EDF} angle and the $\overline{FD}$ length, as shown in 3.6. Therefore, once again with the same method but adding now the two angles and with respect to D, we have:

$$F = [F_x, F_z] = \begin{cases} F_x = D_x + \overline{FD}\cos\left(\alpha_{DE_x} + \alpha_{EDF}\right) \\ F_z = D_z + \overline{FD}\sin\left(\alpha_{DE_x} + \alpha_{EDF}\right) \end{cases} \tag{3.18}$$

Finally, we can move to the last remaining component, the bucket. Point H, the bottom attachment with the boom has already been computed so, point G, the bucket tip location and the bucket angle are the last information required.
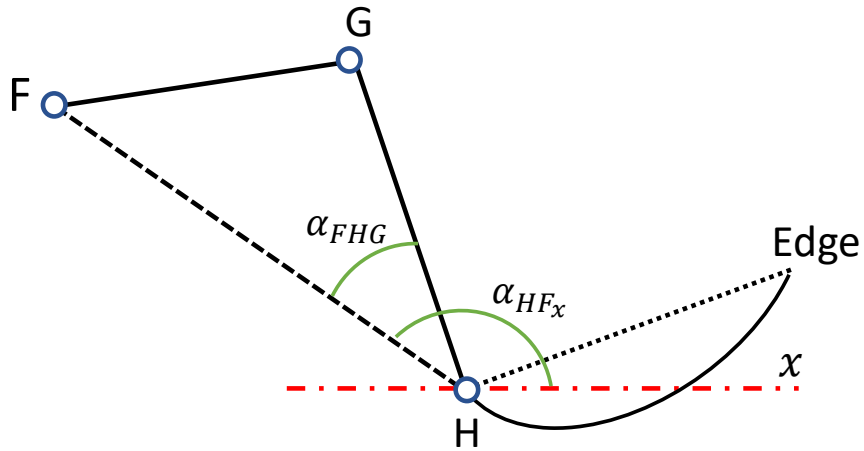
FIGURE 3.7: Angles and triangles for G computation

Once again, since both H and F are known, by using the atan2 function we can directly compute α_{HF_x} and, being angle α_{FHG} computable too (Fig. 3.7), we obtain point G

location as:

$$G = [G_x, G_z] = \begin{cases} G_x = H_x + \overline{GH}\cos\left(\alpha_{HF_x} - \alpha_{FHG}\right) \\ G_z = H_z + \overline{GH}\sin\left(\alpha_{HF_x} - \alpha_{FHG}\right) \end{cases} \tag{3.19}$$

As shown in Fig. 3.8, due to the mechanical design of the bucket, we do not have a null bucket angle when $H_x = G_x$, that is to say there is an offset angle that has to be considered also in here. Then, the bucket angle can be computed as:
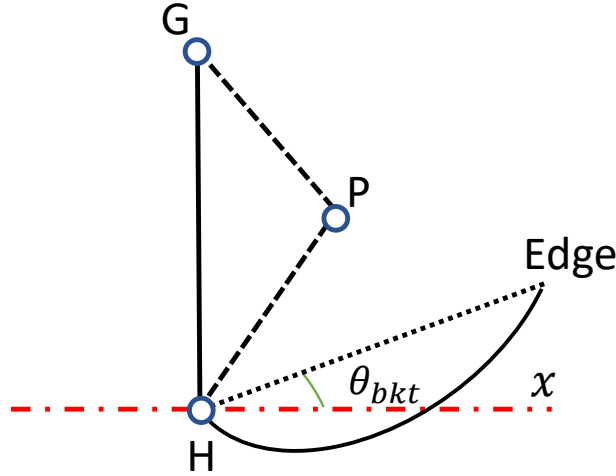
FIGURE 3.8: Bucket geometry and angles needed

$$\theta_{bkt} = \alpha_{HF_x} - \alpha_{FHG} - \alpha_{HG0} \tag{3.20}$$

where:

$$\alpha_{HG0} = \tan^{-1}\left(\frac{425.8}{43.3}\right) \cong 84.19\,\text{deg} \tag{3.21}$$

is the absolute value from H to G when the bucket plate is parallel to the ground (offset angle among x axis). Finally, the bucket edge location can be found, taking into account its own offset angle:

$$\alpha_{HEdge0} = \tan^{-1}\left(\frac{-0.28}{1.26}\right) \cong -12.53\,\text{deg} \tag{3.22}$$

therefore, we have:

$$Edge = [Edge_x, Edge_z] = \begin{cases} Edge_x = H_x + \overline{HEdge}\cos\left(\theta_{bkt} - \alpha_{HEdge0}\right) \\ Edge_z = H_z + \overline{HEdge}\sin\left(\theta_{bkt} - \alpha_{HEdge0}\right) \end{cases} \tag{3.23}$$

Now, as stated before, even if they are just going to be used on the static force analysis
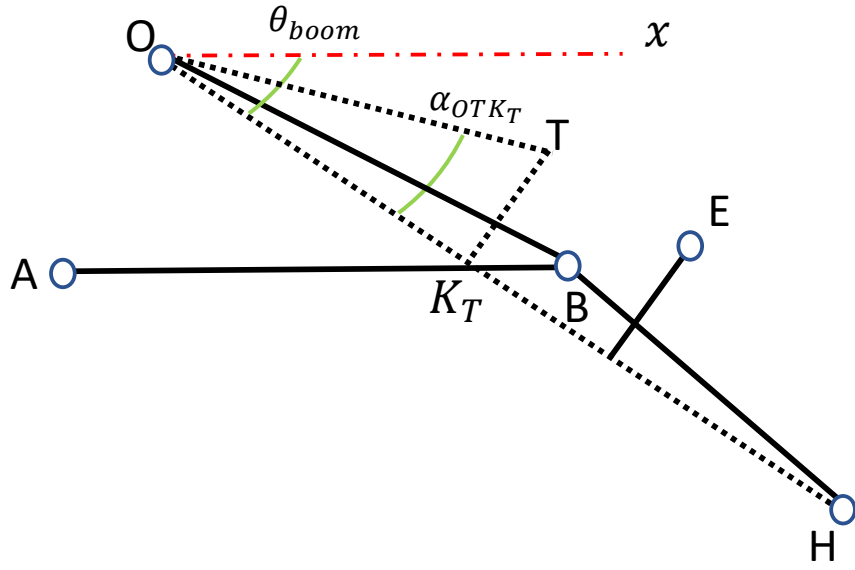
FIGURE 3.9: Angles and triangles for T computation

section, the boom and bucket center of gravity T and P, respectively, are computed as follows: T lies on the boom at a certain height with respect to the line $\overline{OH}$. So, its computation is basically the same done for points E and B:

$$T = [T_x, T_z] = \begin{cases} T_x = \overline{OT}\cos\left(\theta_{boom} - \alpha_{OTK_T}\right) \\ T_z = \overline{OT}\sin\left(\theta_{boom} - \alpha_{OTK_T}\right) \end{cases} \tag{3.24}$$

In Fig. 3.9 the overview of the trigonometry needed and solved is shown. Regarding the bucket center of gravity P, it rotates around hinge H with a radius $\overline{HP}$ (Fig. 3.10).
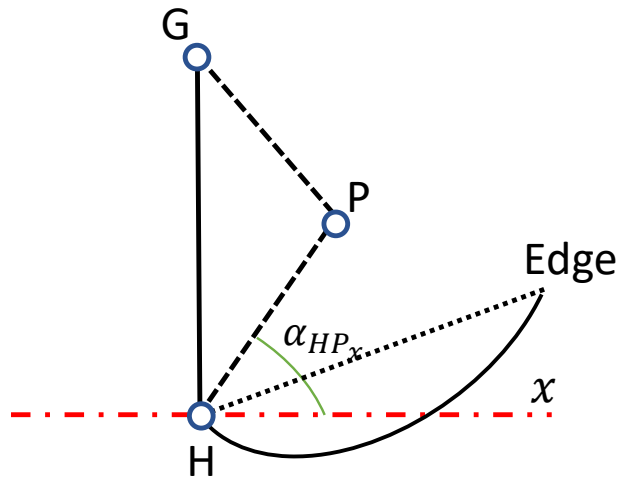
FIGURE 3.10: Angles and triangles for P computation

Therefore, P is almost known a priori. It is easily computable as:

$$P = [P_x, P_z] = \begin{cases} P_x = H_x + \overline{HP} \cos\left(\alpha_{HP_x}\right) \\ P_z = H_z + \overline{HP} \sin\left(\alpha_{HP_x}\right) \end{cases} \tag{3.25}$$

where α_{HP_x} is computable since both the other two points of the rotating triangle are known, being those H and G.

The whole system geometry is now achieved. All the points are expressed as function of either just the boom or both the boom and bucket angles, recalling equations 3.2 and 3.4, depending if they belong just to the boom or not.

Since now the point locations are given, we can take into consideration the reaction forces (along x and z axes) to the hinges and begin with the force balances.

3.4   Static Force Analysis

The purpose of this section is to explain how intensively the hydraulic actuators support the system during non-digging operations, that is to mean, which are the forces at the cylinders for different configurations in order to keep the system steady at that position. In first place, for every hinge shown in Fig. 3.1, an horizontal and a vertical reaction force is considered. Weights are hereby added too. Therefore, boom, bellcrank and bucket centers of gravity now are characterized by a vertical force acting on them given by:

$$\vec{W_{boom}} = M_{boom}\,\vec{g} \quad [\text{N}] \tag{3.26}$$

$$\vec{W_{bell}} = M_{bell}\,\vec{g} \quad [\text{N}] \tag{3.27}$$

$$\vec{W_{bkt}} = M_{bkt}\,\vec{g} \quad [\text{N}] \tag{3.28}$$

where M_{boom} and M_{bkt} represent, respectively, boom, bellcrank and bucket weight in kilograms; $\vec{g}$ is the gravity acceleration vector:

$$\vec{g} = -9.81\,\vec{z} \quad \left[\frac{m}{s^2}\right] \tag{3.29}$$

Starting from the bucket, moving to the bellcrank and finally to the boom, we can compute the reaction force, as x and z terms composition, at every point in the system. The reaction forces at points D and B will be nothing less then the actuating forces demanded by the actuators, respectively, by the tilting and lifting one. A few assumptions are made in order to slightly simplify the system: as stated before, the linkage $\overline{FG}$ weight is neglected,

therefore, the force seen at point F will be exactly equal in magnitude and opposite in verse at point G, that is to say link $\overline{FG}$ is considered as a two-force member. Frictional and inertial effects are neglected too since we can suppose that the implement movements are very slow or at constant velocity ($\longrightarrow a \approx 0$, thus $I \approx 0$) and, since in our research we work with a 16 tons machine, the forces exchanged at the hinges would be so much higher with respect to the frictional effects that these could be neglected too. Finally, we suppose the machine always on a perfect even ground condition, otherwise some of the angles computed in the model would not always be completely accurate and the gravity vector $\vec{g}$ would not reflect the physics properly. Besides, regarding the cylinder forces and the one on F and G, since we know the direction among which the force is transferred (mechanical fixed link), we will have just one unknown since there is a mathematical direct relation between the vertical, the horizontal force and their respective angle, as shown in Fig. 3.11:
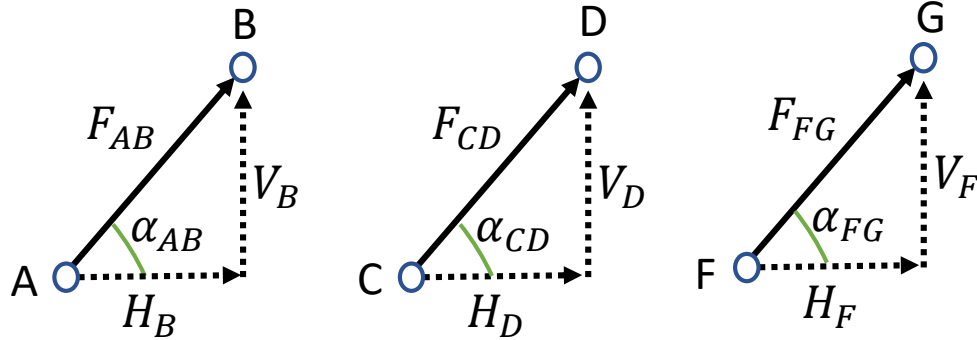
FIGURE 3.11: Mechanical relation between cylinders and link force and their respective angle

where it is possible to state that:

$$V_B = H_B \tan(\alpha_{AB}) \tag{3.30}$$

$$V_D = H_D \tan(\alpha_{CD}) \tag{3.31}$$

$$V_F = H_F \tan(\alpha_{FG}) \tag{3.32}$$

Under these assumptions, we can now start solving the three system of equations, one for each subsystem. In Fig. 3.12 is shown the first balance that has to be solved. Noteworthy that for this section the external forces F_x and F_z acting at the bucket center of gravity P are here null, meaning that we are just computing the forces for non-digging operations. The necessity of their presence will be explained in 3.5, where the model goal is going to be actually evaluate an estimate of those two external forces depending on the geometric configuration and on the hydraulic cylinders pressures. Therefore, we can write the first
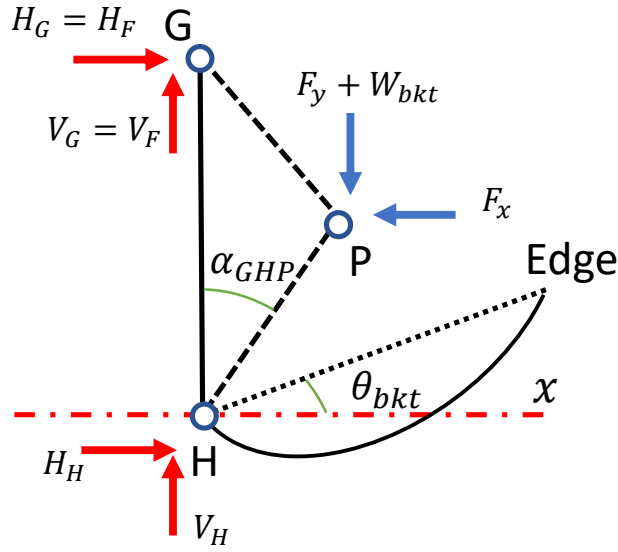
FIGURE 3.12: Bucket balance

system of equation:

$$\begin{cases} \sum_x & H_F + H_H = 0 \\ \sum_z & H_F \tan(\alpha_{FG}) + V_H = W_{bkt} \\ \stackrel{\frown}{H} \quad \overline{HG} \; H_F\big(\tan(\alpha_{FG})\cos(\alpha_{HG}) - \sin(\alpha_{HG})\big) = \overline{HP}\, W_{bkt}\cos(\alpha_{HP}) \end{cases} \tag{3.33}$$

thus, by solving for the unknowns H_F, V_H and H_H, recalling 3.32, we can calculate the reaction forces on hinges F and E. These forces become known values that will be used for the other two remaining balances. Thus, we can move one step forward to the bellcrank balance shown in Fig. 3.13:
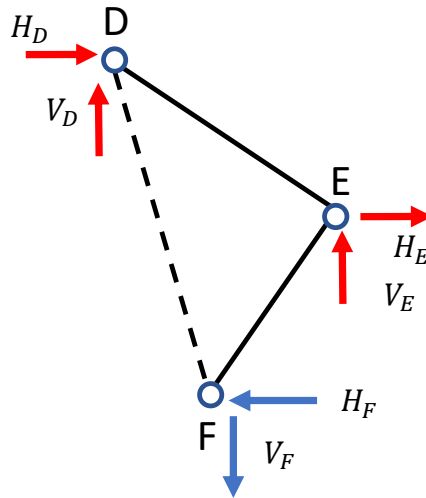
FIGURE 3.13: Bellcrank balance

It is notable how the reaction forces in point F are now known values with opposite verse with respect to Fig. 3.12 due to the aforementioned properties of the fixed link $\overline{FG}$. Thus, we obtain:

$$\begin{cases} \sum_x & H_D + H_E = H_F \\ \sum_z & H_D \tan(\alpha_{CD}) + V_E = W_{bell} + V_F \\ \widehat{E} & \overline{ED}H_D\big(\tan(\alpha_{CD})\cos(\alpha_{ED}) - \sin(\alpha_{ED})\big) = \overline{EF}\big(V_F\cos(\alpha_{E}F) - H_F\sin(\alpha_{EF})\big) = 0 \end{cases}$$
$$(3.34)$$

where, recalling the assumption we made about the bellcrank center of gravity, the
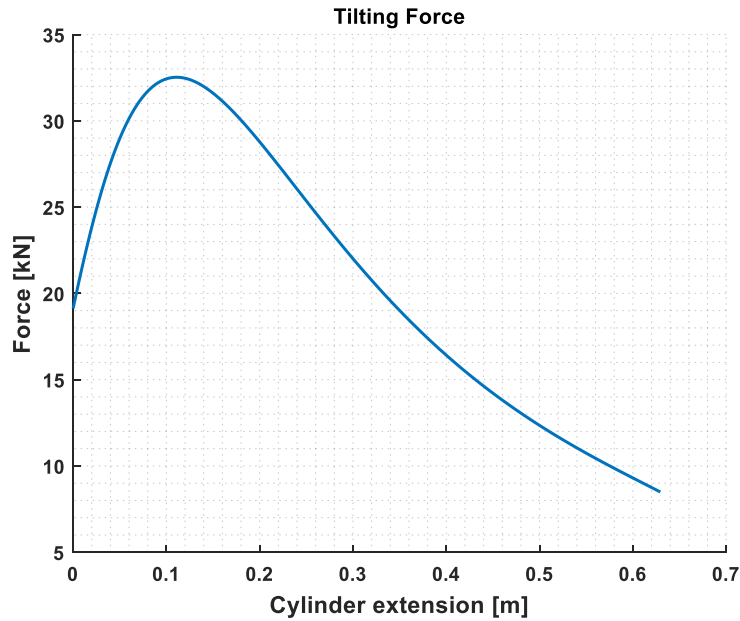
FIGURE 3.14: Tilting cycle with lift cylinder extension fixed at 0.5m

moment balance equation around E can be impose equal to zero. Therefore, thanks to equation 3.31, we achieve the force demanded by the tilting hydraulic actuator, as we can see in Fig. 3.14, where a tilting cycle is performed keeping a fixed lifting cylinder extension at 0.5m (arbitrary value chosen just to shown the trend of the demanded tilting force). As we can see, the curve is increasing until it reaches a maximum (cylinder extension is at ≈ 0.1 m): this is because the bucket center of gravity during a tilting phase moves among a circumference centered in H with $\overline{HP}$ as radius. The maximum force is demanded when the center of gravity is at the furthest distance with respect to H. After that, P gets closer to H from the top part and the required tilting force from the actuator starts decreasing (the load enters in a semi-overrunning configuration where its force and its velocity contribute to the tilting).

The reaction forces on E found from 3.34 are now used as known values for the last system of equations, the one on the boom, as shown in Fig. 3.15:
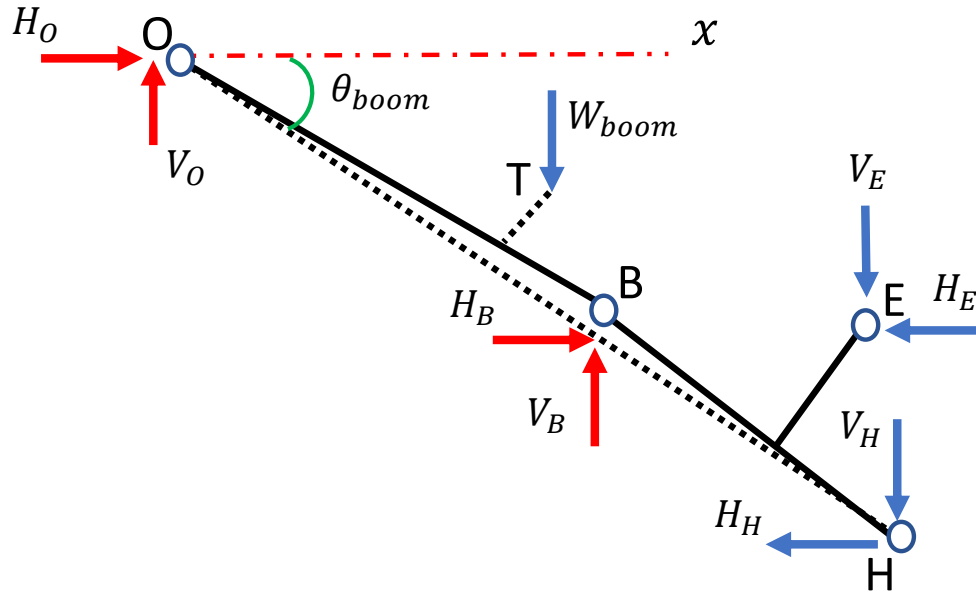
FIGURE 3.15: Boom balance

$$
\begin{cases}
\sum_x & H_O + H_B = H_E + H_H \\
\sum_z & H_B \tan(\alpha_{AB}) + V_O = W_{boom} + V_E + V_H \\
\overset{\frown}{O} & \overline{OB}H_B\big(\tan(\alpha_{AB})\cos(\alpha_{OB}) - \sin(\alpha_{OB})\big) = \overline{OT}W_{boom}\cos(\alpha_{OT}) + \overline{OH}\big(V_H\cos(\theta_{boom}) - \\
& -H_H\sin(\theta_{boom})\big) + \overline{OE}\big(V_E\cos(\alpha_{OE}) - H_E\sin(\alpha_{OE})\big)
\end{cases}
$$

$$(3.35)$$

By solving this system, we finally obtain the reaction force on hinge O and the forces
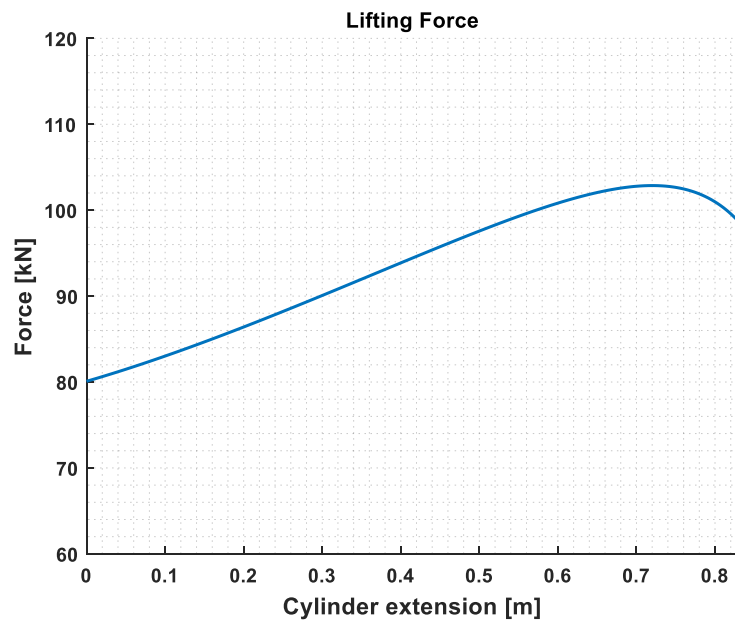
FIGURE 3.16: Tilting cycle with tilt cylinder extension fixed at 0.4m

required by the lifting cylinders. Since our computations are made in a two-dimensional plane but we actually have two lifting actuators, the force demanded by each of them is going to simply half of the one given by 3.35. In Fig. 3.16 we can see how the total lifting force curve, over L_1 extension, is increasing as the cylinder extends until it reaches a semi-plateau where the lifting phase is simulated keeping a fixed tilt cylinder extension at 0.4m.

3.5   External Force Estimate

Section 3.4 described how, for every possible implement position, the system in Fig. 3.2 is able to compute the force required by the actuators to balance the steady state configuration. Another fundamental goal of this research was, by inverting the procedure just illustrated, meaning that we start from the geometric configuration and the forces at the actuators, obtain an estimate of the external forces acting at the bucket center of gravity P. Thus, our new reference system is shown in Fig. 3.17:
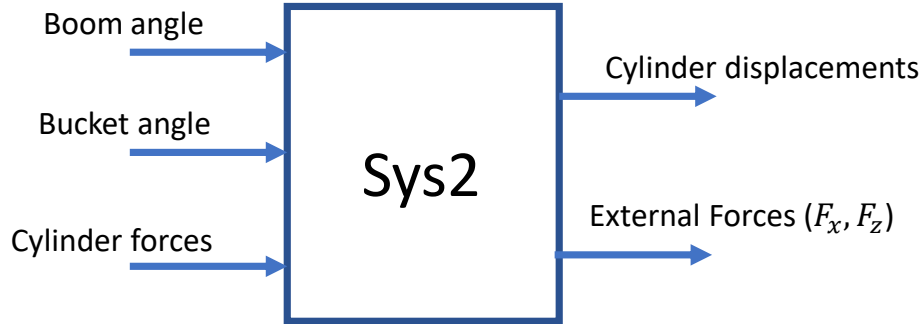
FIGURE 3.17: Bellcrank inverse balance

The methodology for obtaining all the reaction forces and, consequently, the payload and horizontal force estimate, is similar as before: two system of equations are solved. The bellcrank subsystem is the first one to be resolved (Fig. 3.18). It is noticeable how now the known values are the component weight and the force provided by the hydraulic actuator and the unknowns are the forces at hinges E and F. Consequently, we can solve the following system of equations, recalling 3.32, for the unknowns V_E, H_E and H_F:

$$\begin{cases} \sum_x \quad H_F - H_E = H_D \\ \sum_z \quad H_F \tan(\alpha_{FG}) - V_E = V_D - W_{bell} \\ \widehat{E} \quad \overline{EF} H_F\big(\sin(\alpha_{EF}) - \tan(\alpha_{FG})\cos(\alpha_{ED})\big) = \overline{ED}\big(V_D\cos(\alpha_E D) - H_D\sin(\alpha_{ED})\big) = 0 \end{cases}$$

$$(3.36)$$
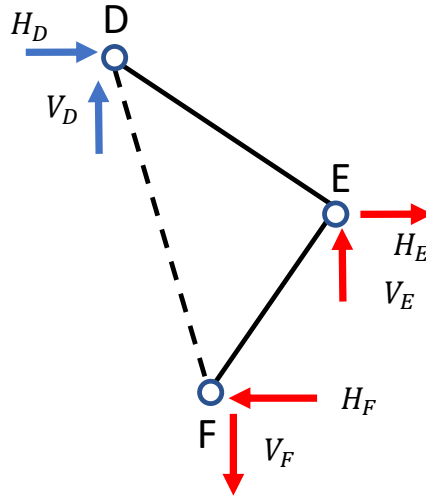
FIGURE 3.18: Bellcrank inverse balance

The situation for the other system of equations is slightly more intricate since boom and bucket balances need to be solved simultaneously, as shown in Fig. 3.19:
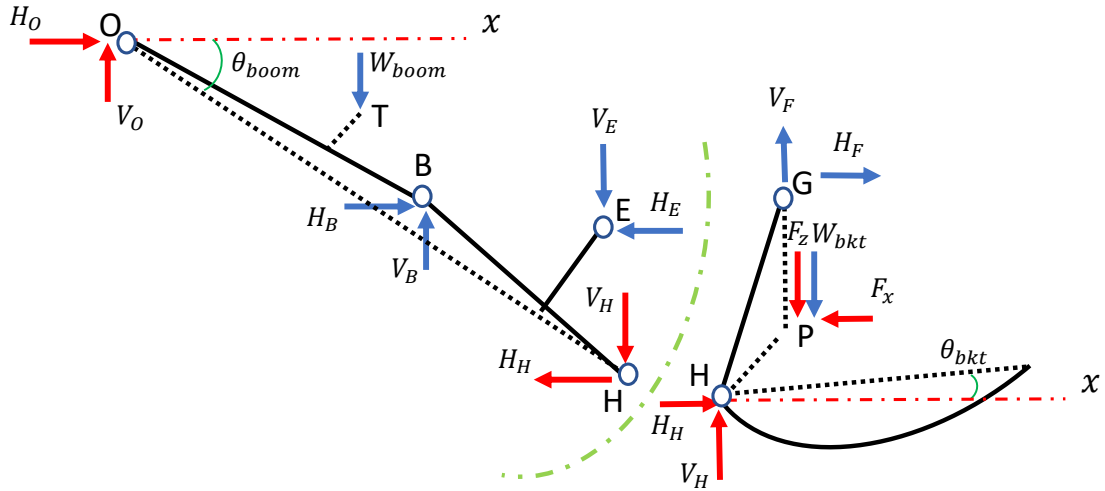
FIGURE 3.19: Boom and bucket simultaneous balance

This is because if we moved directly to solve just the boom balance, we would wind up with a statically indeterminate system since we would have four unknowns (V_O, H_O, V_H and H_H) in just three equations (vertical, horizontal and moment balance). A solution to this problem relies in solving boom and bucket balances as one, since reaction forces on H are inter exchanged between the two components, achieving six equation is six unknowns. Hence, a 6×6 matrix is constructed and solved for the unknown values V_O, H_O, V_H, H_H, F_x and F_z, taking into account that the forces at F and E have already been computed

from 3.36:

$$
\begin{cases}
\text{Boom:} \\
\sum_x \quad H_O - H_H = H_E - H_B \\
\sum_z \quad V_O - V_H = V_E + W_{boom} - V_B \\
\widehat{O} \quad \overline{OH}H_H \sin(\theta_{boom}) - V_H \cos(\theta_{boom}) = \overline{OT}W_{boom}\cos(\alpha_{OT}) - \overline{OB}\big(V_B\cos(\alpha_{OB}) - \\
\quad - H_B\sin(\alpha_{OB})\big) + \overline{OE}\big(V_E\cos(\alpha_{OE}) - H_E\sin(\alpha_{OE})\big) \\
\text{Bucket:} \\
\sum_x \quad H_H - F_x = -H_F \\
\sum_z \quad V_H = W_{bkt} - V_F \\
\widehat{H} \quad \overline{HP}\big(F_z\cos(\alpha_{HP}) - F_x\sin(\alpha_{HP})\big) = \overline{HP}W_{bkt}\cos(\alpha_{HP}) + \overline{HG}\big(H_F\sin(\alpha_{HG}) - V_F\cos(\alpha_{HG})\big)
\end{cases}
$$

$$(3.37)$$

In order to check the consistency and correctness of our equations in a very simple way, i run a co-simulation between the code implementing system 3.2 and the one implementing 3.17.
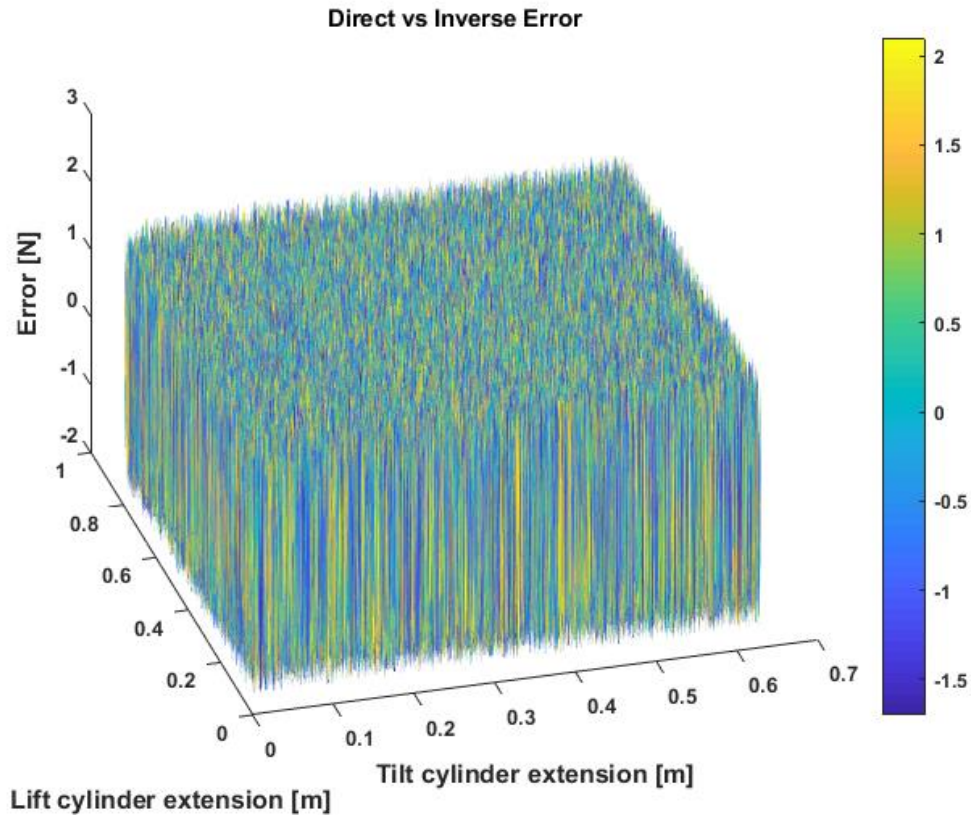
FIGURE 3.20: Error between direct and inverse computation on F_z

Clearly, since i am imposing a null external force along the x and z axes for section

3.4, i am expecting null or very low force at the bucket center of gravity for the second system. That being said, i am here basically computing the actuator forces for a certain configuration and inputting those in the inverse procedure method to double check for null forces at the bucket. Fig. 3.20 shows the expected result: the external forces are oscillating among zero with a maximum amplitude of 2N (meaning a mass of $\approx$ 200gr) clearly brought by intern numerical errors of the CPU. The horizontal estimate results are exactly equivalent to the vertical ones, where another heavy oscillating force is witnessed for the whole simulation.

Chapter 4

Numerical Model

The goal of this section is to introduce the methodology used for the design and realization of a complementary numerical model. Starting from the software environments and tools used, the focus moves into how the CAD files have been generated starting from just essential data provided by the sponsor that donated the machine used for my research. The attention is finally moved into the actual generation of the Simulink file containing the numerical model: a few operations were needed in order to exploit its powerfulness, such as commanding the implement motion, sensing positions, velocities, accelerations, forces, etc. as it is going to be expressed later on.

4.1   Methodology

In order to validate and double check the analytical model, a numerical solution has been designed through the utilization of MATLAB/Simulink environment. The Simmechanics/Simscape toolbox can generate automatically a numerical model by importing three-dimensional files of the components: therefore, this was the methodology key for the numerical model generation. The creation of a CAD file for each part composing the implement was performed starting from a file given by the sponsor containing all the geometric properties needed: distance between the hinges, center of gravity of the different implement components, material properties and inertia matrices. All the individual parts are consequently matched into a single system through an assembly phase. With respect to section 3.4, in here there was no need to simplify the system with the simplification assumptions made before since, taking into consideration the fact that our model is not so complex/non-linear, the solution is completely provided by the Simmechanics toolbox. Therefore, the main difference between analytical and numerical model relies on

weights: the link and actuators masses are here considered. The only assumption still valid is neglecting inertial components since also for the numerical model i ran relatively slow motion simulations ($a \cong 0 \longleftrightarrow I \cong 0$). Hence, what we are expecting from the numerical model simulations is to see, with respect to the analytical one, a positive offset on the demanded actuating forces that is brought by the small (but still present) weight difference between the two systems.

4.2 3D Model Generation

The CAD file generation has been performed through SolidWorks software environment. A total of nine components was designed: chassis, essential for the boom and hydraulic actuators attachments, boom, bellcrank, link, bucket, lifting and tilting cylinders (each of them composed by case and rod).
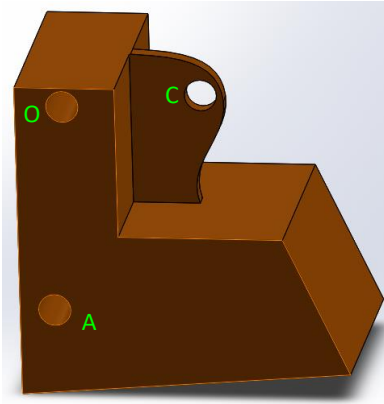
FIGURE 4.1: CAD file of the chassis

The main problem to face for the CADs design was that, since several classified information about the sponsor machine were involved, all the components had to be realized starting from zero and without any reference to the machine used. Therefore, a very basic and simplified version of the above mentioned components have been made with maximum priority in keeping the point distances to the desired values. Material properties and inertia matrices data were not used but, after the completion of the component, centers of gravity and mass properties were overridden to the desirable values. Doing so, we wind up having a completely unrelated (in terms of shape and sponsor logos) system, with respect to our reference machine, behaving exactly as it. The chassis, shown in Fig. 4.1, is the first

component developed: As we can clearly see, the shape of the part is heavily simplified
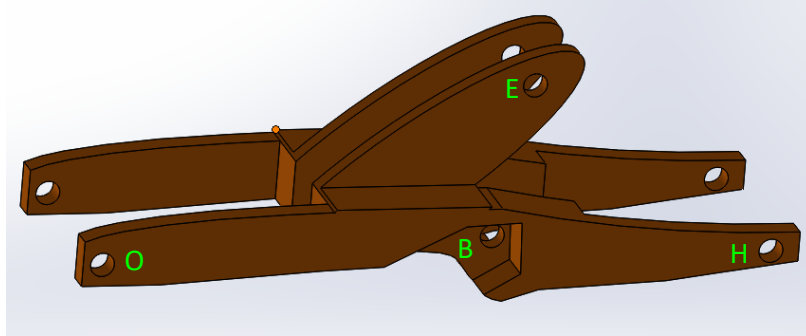
FIGURE 4.2: CAD file of the boom

but again, the purpose here was having a similar shape but exact properties component. Recalling 3.1, we can highlight points O, A and C, being, respectively, boom-chassis attachment, lifting and tilting cylinders chassis attachments. The second component is the boom, as shown in Fig. 4.2: where we can clearly distinguish point O, B, E and H.
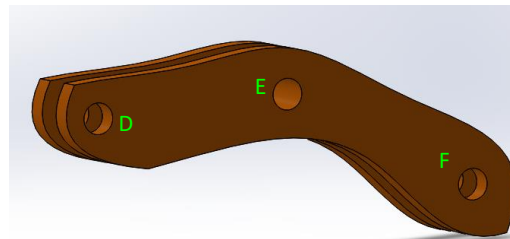
FIGURE 4.3: CAD file of the bellcrank

All the points inter exchanged between the components are subsequently matched during

the assembly phase. In Fig. 4.3 the bellcrank is shown, where the center point E does not match any more with its center of gravity (even if the difference is still significantly small), as it was assumed for the analytical model. Tilting rod D and link F attachments are highlighted. After that, due to its extremely simplicity, the link is the only component reflecting very precisely the actual shape, as shown in Fig. 4.4. Besides point F, exchanged
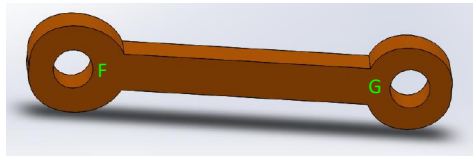
FIGURE 4.4: CAD file of the link

with the bellcrank, point G is highlighted. The last component is shown in Fig. 4.5, where
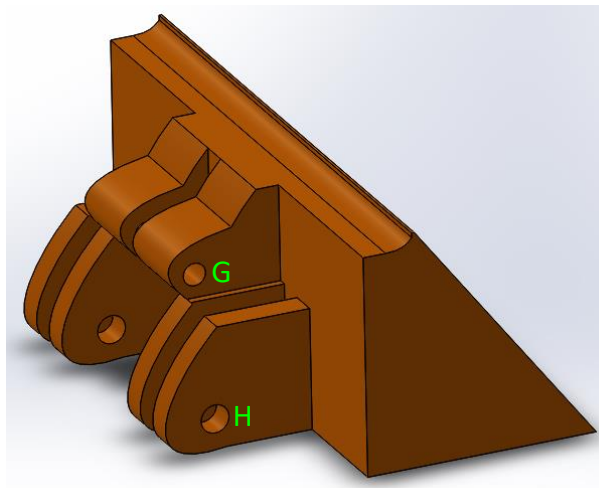
FIGURE 4.5: CAD file of the bucket

the bottom holes correspond to the boom attachment H and the top ones are for the link one.

Finally, in Fig. 4.6 we can see the hydraulic actuators developed for the numerical model: in the top image the lifting actuator with its chassis-boom attachments, respectively A and B, is shown. In the bottom picture the tilting cylinder with its chassis-bellcrank attachments, respectively C and D, is shown.

(a) Lift cylinder
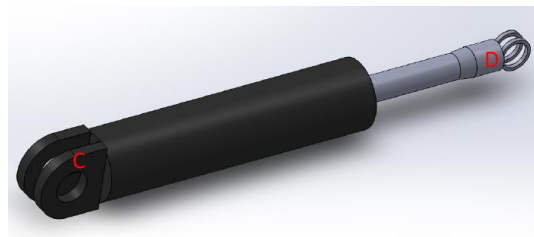
(b) Tilt cylinder

FIGURE 4.6: CAD files of hydraulic actuators

Once all the necessary components are developed, the matching phase to compose a single assembly file takes place. Without going into much details for the several matches needed for the parts, the overall system is shown in Fig. 4.7.
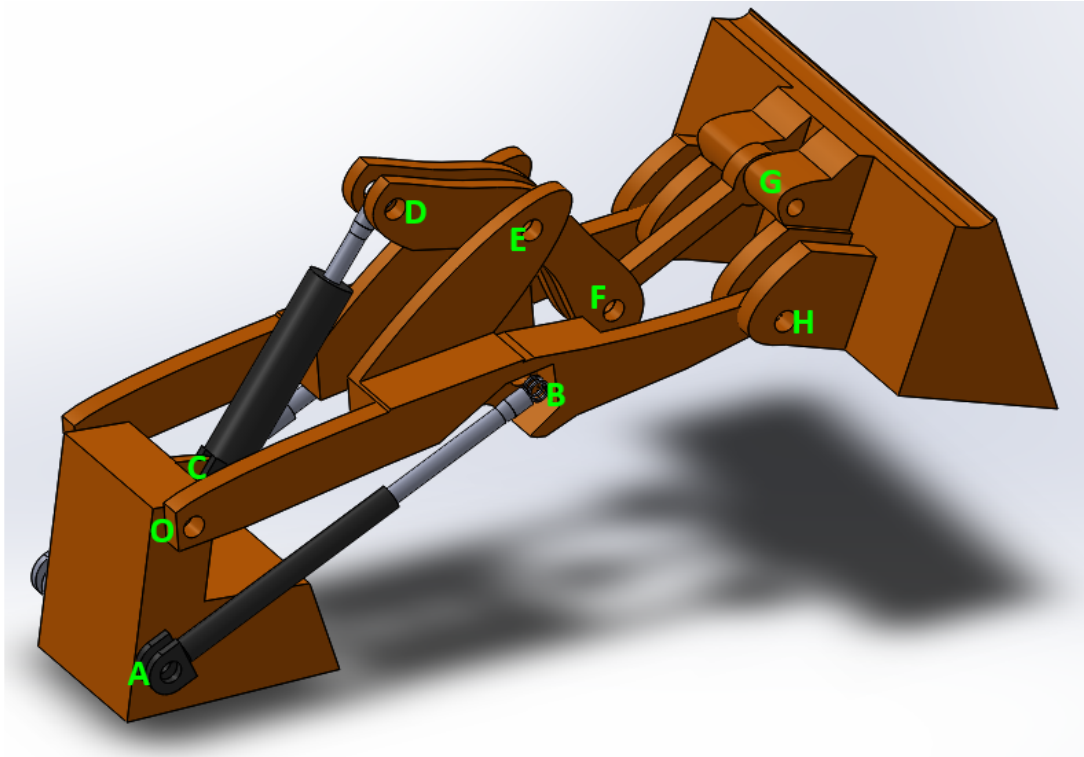
FIGURE 4.7: CAD file of the overall assembled system

It is just worth of mention that all the mates needed for the assembly file are performed in order to reflect the physics behavior of the real-world machine (e.g. rods staying inside the cases, non-overlapping components, etc.). Everything is now ready for the actual numerical model generation.

4.3   Model Architecture

Once the three-dimensional file of the system has been created, the numerical model can finally be generated. The MATLAB/Simulink environment is used: in order to have the softwares (MATLAB and SolidWorks) able to inter exchange data between them, the Sim-Mechanics Link toolbox (with the proper version of MATLAB running on the computer) has to be downloaded from Mathworks website:

https://www.mathworks.com/products/simmechanics.html

then, in order to install the add on, a few operations have to take place. First of all, the downloaded files from the Mathworks website will be a *.zip* and a *.m*. Thereafter, the first operation, that has to be performed as computer administrator, is the following:

$$\texttt{install\_addon(smlink.r2018a.win64.zip)} \tag{4.1}$$

where again it varies depending on the MATLAB version, the computer operating system (Windows, UNIX or Mac OS) and architecture type (32 or 64 bits) used. To finally connect the two pieces of software another function has to be run:

$$\texttt{regmatlabserver} \tag{4.2}$$

which basically registers the current MATLAB executable as automation server. The final step remaining is enabling the Simscape MultiBody Link plug-in, through:

$$\texttt{smlink\_linksw} \tag{4.3}$$

Now, if everything has been completed successfully without errors, in the add-ins section of SolidWorks, being in the tool section of the menu bar, the SimMechanics Link option should be available. Therefore, through its usage, an *.xml* file representing the system components with their respective weights, properties and matches, is created. Consequently, the Simulink model is generated through:

$$\texttt{smimport(multibodyDescriptionFile)} \tag{4.4}$$

where 4.4 expresses the function used to perform the import of the multi body description file into MATLAB environment. In Fig. 4.8 we can see the overview of the Simulink system after the import operation: where in light blue background the different single components are highlighted. The several cylindrical and revolute joints are automatically created by Simscape depending on the matches properties given from SolidWorks. Some additional blocks were needed in order to import simulation data to MATLAB for processing; besides, some adjustments for the calibration of the angles and cylinders displacements computation were included, as shown in Fig. 4.9:
where it is noticeable how the complexity of the overall system, with respect to 4.8, has considerably increased. The sets of blocks going into the cylinders hinges, both on the lifting and the tilting, are strictly necessary and used for simulation purposes. To those hinges, a motion (position) control simulation is performed; the other big sets of blocks are used for calibration and storage purposes. From th cylinders joints, the extension displacement is firstly measured and managed for storing data into MATLAB workspace.

FIGURE 4.8: Bare Simulink numerical model

Same reasoning stays for boom and bucket angles: after a radians-degrees conversion and a calibration, the data is stored into MATLAB workspace for post processing operations. The simulations ran with the numerical model were performed by inputting the motion desired (both cylinder displacement extensions) and their respective first and second derivatives (velocity v and acceleration a of the rods): Simscape thereafter automatically computed the forces required by the hydraulic actuators in order to have the desired motion trajectory.

FIGURE 4.9: Simulink numerical model

Chapter 5

Results and Validation

The main purpose of this chapter is to explore the results obtained throughout the analytical and numerical models developed. Simulations were run and output data is here compared and discussed. Furthermore, in-field data has been collected from experimental tests: the final comparison is therefore performed between both the simulated models and data coming from the reference machine. Here an explanation on what was expected and what was achieved is also carried out.

5.1 Simulation Model Comparison

The first section of this chapter aims in checking a match between analytical and numerical model, The comparison criteria relies on both kinematic and dynamic quantities. All the data coming from the numerical model developed with Simscape is exported, for every simulation, into MATLAB for easier and faster post processing operations. The solver configuration parameters for Simulink simulations are here expressed:

$$
\begin{cases}
\text{Initial and final time} \quad \longrightarrow \quad T_i = 0 \text{ s} \quad T_f = 8 \text{ s} \\
\text{Type: Fixed-step with Automatic solver selection} \\
\text{Fixed-step size (fundamental sample time)} \quad \longrightarrow \quad T_s = 5 \text{ ms}
\end{cases}
\tag{5.1}
$$

therefore the simulation window time $\Delta T = 8$ s with a sampling frequency of $f_s = 200 H_z$ generates time-vectors of 1600 elements. Regarding the analytical model, two MATLAB function has been generated for simulation purposes:

$$[\theta_{boom}, \theta_{bkt}] = \texttt{kin} \left(L_{1ex}, L_{2ex} \right) \tag{5.2}$$

$$[F_{AB}, F_{CD}] = \texttt{dyn} \left(L_{1ex}, L_{2ex} \right) \tag{5.3}$$

Firstly, the geometry ascertainment is realized: boom and bucket angles of the two models are compared for every reachable configuration. Recalling equations 3.2 and 3.4, we will have a two-dimensional plot comparison for the boom angle (since it is strictly related just from the lifting cylinder extension L_{1ex}) and a three-dimensional surface plot for the bucket angle (since it is strictly dependent from both tilting and lifting cylinder extensions, L_{2ex} and L_{1ex}, respectively). The two angle comparisons have been carried out as follows: the first simulations were done in Simulink, through the use of Simscape; then, since all the data is stored in the MATLAB workspace, the cylinder displacements have been inputted in equation 5.2 (and in 5.3 for the force comparison). The output has been thereafter compared with the one coming from Simulink; doing so, we achieved a perfect input correspondence. Therefore, for the boom angle comparison, the lifting cylinder is extended from null to maximum stroke, no matter the tilting cylinder extension (kept constant at 0.5m here). Thus, throughout the use of function 5.2, as shown in Fig. 5.1, we obtain two overlapping curves in the two-dimensional plot:
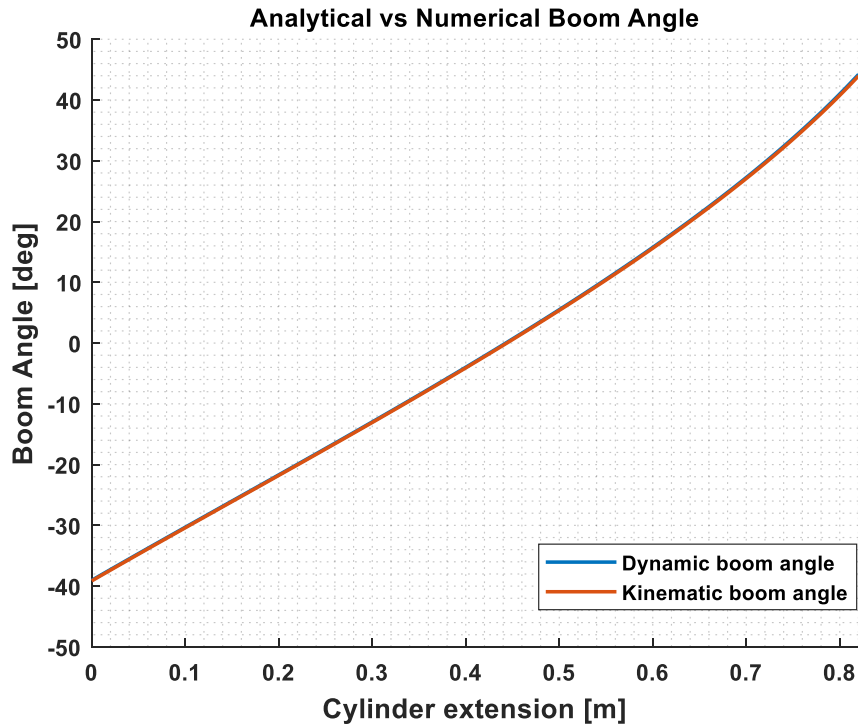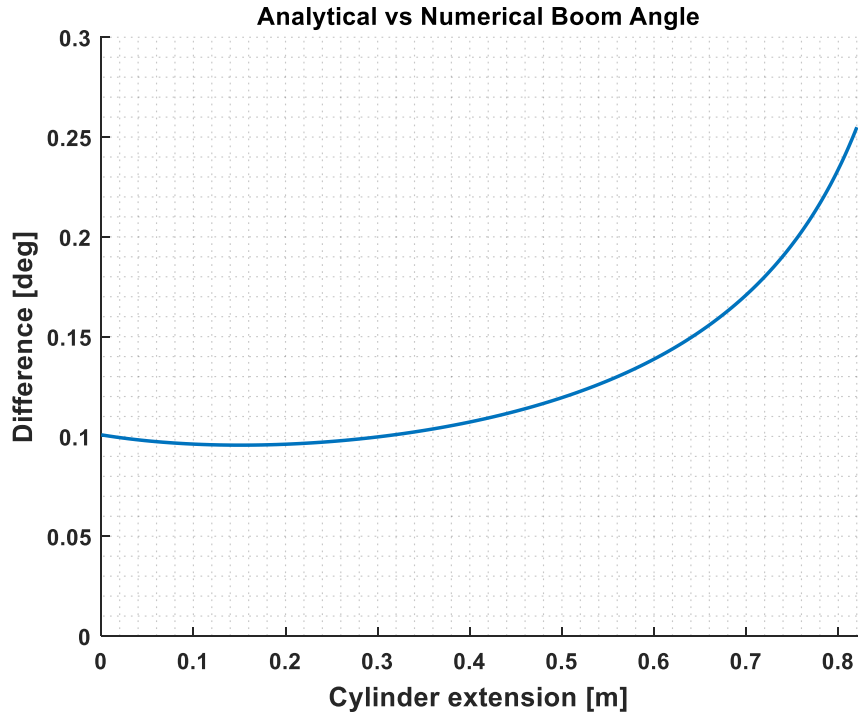

FIGURE 5.1: Analytical vs Numerical boom angle plot over L_{1ex}

where it is pretty neat how the behavior of both the curves is basically identical. In fact, as shown in 5.2, the difference between the models is negligible:

FIGURE 5.2: Analytical vs Numerical boom angle difference plot over L_{1ex}

where a maximum "error"of ≈ 26 °is achieved. We cannot really talk about error here because we do not have a reference model that we know for sure is right (even if most likely is the analytical model from a geometric point of view), hence, the term difference is here used. In order to perform this first comparison just one Simulink-Simscape simulation was needed: with the 1600 elements vector containing the lifting cylinder extension coming from it, function 5.2 was run (clearly, for 1600 times).

Slightly more complicated is the bucket angle simulation since it is function of two variables. Therefore, for having comparable data, 1600 Simulink-Simscape simulations were run: a complete tilting phase (from null to maximum stroke) keeping a fixed the lifting cylinder extension (increasing at every iteration from null to maximum stroke). Hence, function 5.2 was run 1600×1600 storing the data in a matrix at every iteration.

Besides, due to mechanical constraints of the reference machine, we have unreachable areas of the surface plot as shown in Fig. 5.3, where the bucket angle surface plot of the analytical model is shown: it is notable how, if we have a null tilting cylinder extension (bucket completely dropped) we can raise the boom until a certain threshold, around ≈ 0.58 m. After that, the lifting phase is locked by mechanical constraints and then, if we want to keep raising the boom, we need to have some extension coming from the tilting hydraulic actuator.

Hence, in our comparison between the two model bucket angles, as shown in Fig. 5.4, we obtain a triangle shaped area not highlighted because those particular configurations cannot be reached.
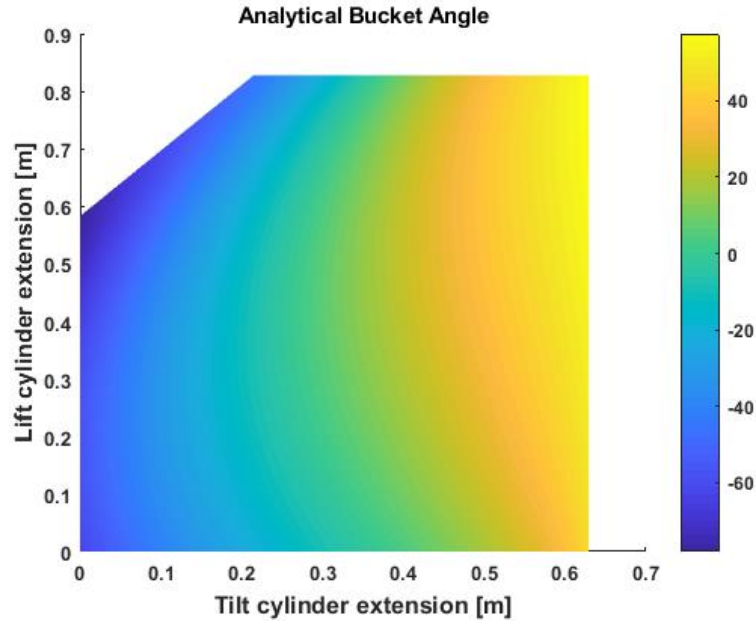
FIGURE 5.3: Analytical bucket angle surface plot over L_{1ex} and L_{2ex}
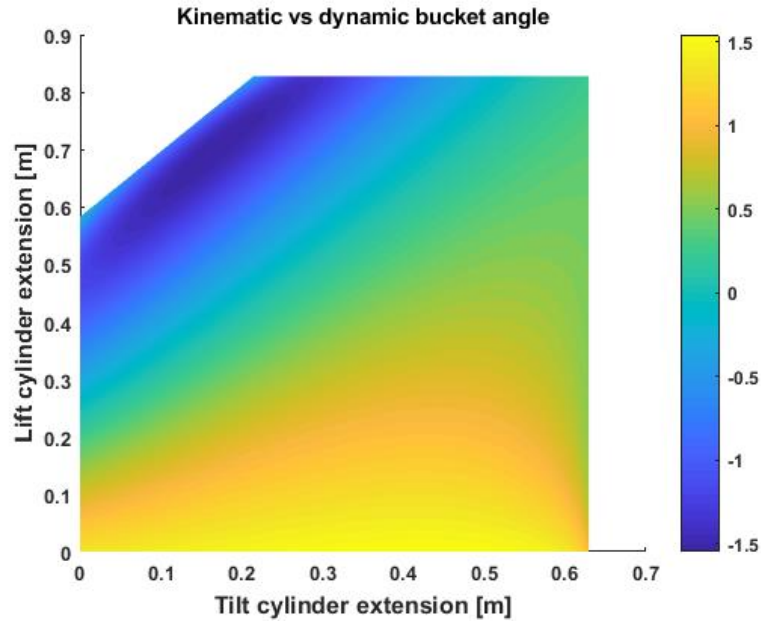
FIGURE 5.4: Analytical vs Numerical bucket angle difference surface plot over L_{1ex} and L_{2ex}

We can notice how, with respect to the boom angle comparison, here we achieve higher difference values, reaching somewhere a maximum "error" of $\approx \pm 1.5$ °. First of all, it should be mentioned that higher differences are reached at extreme configurations: positive high difference for tilting phases with null or very low lifting cylinder extension and negative high difference during the forced transition of lifting phases with null or minimum tilting

cylinder extension (allowing the achievement of reachability for that particular boom position). That being said, in here we also have to consider that the bucket angle computation requires a higher volume of calculations, most of them being non-linear due to presence of sines, cosines, square roots and exponentials, and some part of the "error" could be actually brought by CPU internal errors. Nevertheless, we are still achieving a very acceptable result since for the most part of the surface the difference oscillates between $\approx \pm 0.5$ °, and even where it reaches the highest values, we are still having a negligible discrepancy between the models.

Once we obtained a more then acceptable result for the geometry, and therefore for the point locations, the next step is comparing how the reaction forces behave for both the models. What we expect is to see higher fores on the numerical model for same configurations with respect to the analytical model: due to the absence of the link $\overline{FG}$ and the three hydraulic actuators weights, the analytical model is going to require lower actuation forces on both lifting and tilting phases.

Firstly, the lifting force between the models is compared: the bucket position is not a predominant factor here since its center of gravity modifies in a slight way the overall one. Therefore, a lifting phase simulation with an arbitrary tilting cylinder extension at 0.6 m is run, as shown in Fig. 5.5:
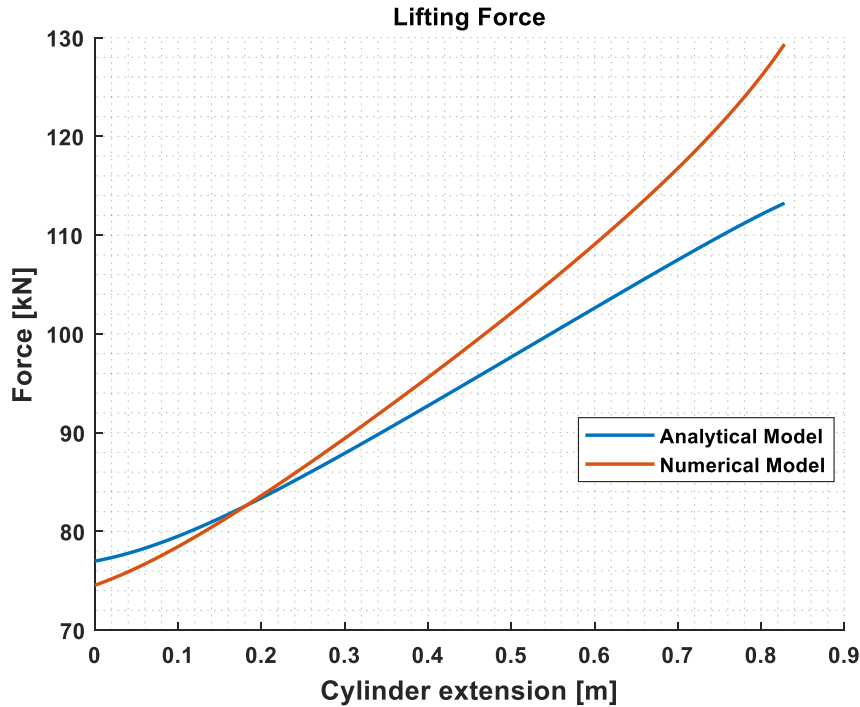
FIGURE 5.5: Analytical vs Numerical lifting force plot over L_{1ex} with a constant $L_{2ex} = 0.5$m

where the curves represent the lifting overall force required to balance the system, being that the force sum coming from both the lifting hydraulic actuators. It is noticeable how

the plot starts with a higher force for the analytical model with an offset of ≈ 1 kN with respect to the numerical model. Nevertheless, by increasing the lift cylinder length we start having a steeper trend for the numerical model until it crosses the line of the analytical one at ≈ 0.2 m. The gap between the curves increases until maximum cylinder extension where a difference of ≈ 15 kN is reached. The overall behavior reflects what expected: the numerical model has higher lifting force values for most part of the available range due to the additional weight non included in the analytical model. The maximum difference of 15 kN is reasonable considering that just the link and cylinder weights are around 620 Kg total. Besides, in the analytical model inertia is not considered and this could be the closing gap between the curves. We can now move forward into the tilting forces comparison: anyways, the assumption made for the lifting phase is here not valid anymore since the boom position heavily influence the magnitude and trend of the required tilting force. In order to solve this problem, three tilting phases with different boom positions were run as shown in Fig. 5.6:

(a) Tilting force at $L_{1ex} = 0.2$ m

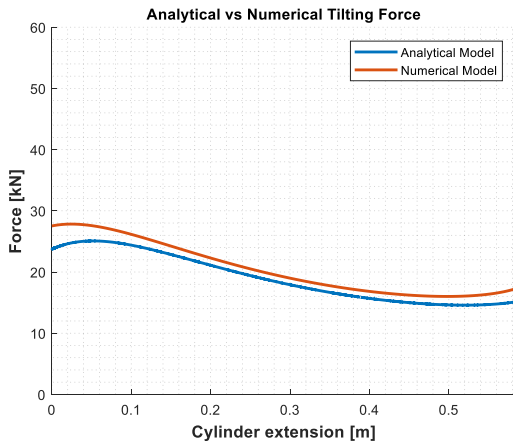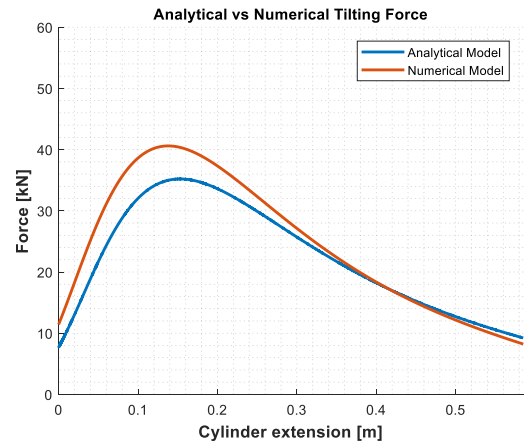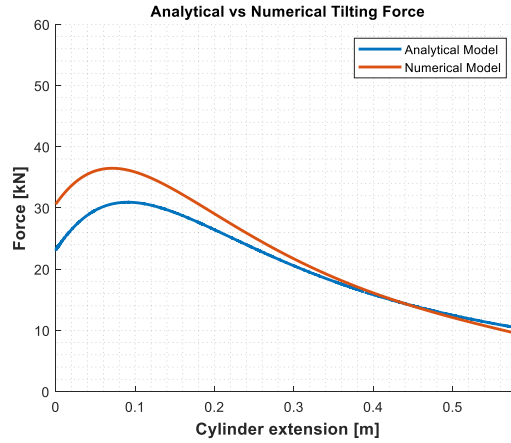(b) Tilting force at $L_{1ex} = 0.4$ m

(c) Tilting force at $L_{1ex} = 0.6$ m

FIGURE 5.6: Analytical vs Numerical lifting force plots over L_{2ex} with a different constants L_{1ex}

First of all, it is notable how, for all the plots, we obtain a very similar behavior between analytical and numerical model, regardless the boom position. Moreover, a higher force is achieved by the numerical model in mostly all the parts of the plots. Moreover, all the plots witness a significantly lower offset between numerical and analytical model. This is due to mainly two reasons: firstly, during a tilting phase, the actuator has to bear just its own weight since the lifting cylinder ones do not influence the tilt actuating force required. Secondly, the $\overline{FG}$ link weight here is just something that the cylinder has to move as a rigid body in order to tilt the bucket and not a weight that has to be supported as was happening for the lifting forces. Furthermore, as it has been shown in Fig. 3.14, also here, more visible in Fig. 5.6(b) and Fig. 5.6(c), the tilting force trend increases steeply from null extension until it reaches a maximum around $L_{2ex} = 0.1 \div 0.15$ m. After that, by keep increasing the cylinder extension, the tilting force required decreases almost linearly. This is due to the bucket center of gravity location during the phase: it moves on a circumference centered in H and radius $\overline{HP}$. With null extension, the center of gravity it is located beneath the hinge H: by increasing the cylinder extension, P starts following the circumference curve until it reaches, with respect to the horizontal axis x, the furtherest distance to H, where the maximum force demanded is reached. After this point, the center of gravity starts getting closer, still with respect to the horizontal axis x, to hinge H but above it, not below as was happening in the tilting phase start: the bucket is now actually helping the tilting operation since its weight is not more completely resistive but, as soon as $P_z \geq H_z$, meaning it crosses the horizontal axis given by the position of H, it becomes semi-overrunning load. That being said, we can finally state that the models match in a very acceptable way also for the tilting cylinder force given by F_{CD}.

5.2 Experimental Setup

In the previous section a solid match between the analytical an numerical simulated models has been achieved. Therefore, the next step is now to move into field test data collection for pursuing experimental comparison match with the simulated ones. Since the lifting and tilting force values in the simulated models are steady state, the goal of this research part is to obtain equal or similar force values for the same geometric configuration keeping the machine implement still. Throughout the use of several sensors, a LABVIEW code developed is able to compute the geometric configuration of the implement and the required forces at the actuators. The reference machine was modified in several ways to create the new functions which were needed to run the tests, as well as adding instrumentation for acquiring the desired data. This section enumerates the various sensors needed and installed on the wheel loader system for the purpose of my research. Nevertheless,

since there are other on-going researches on the reference machine, it is worth to say that several other sensors were already installed on it. Anyways, they will not be listed here since they were not used for the model experimental validation. The table below shows the list of sensor needed and installed:

Sensor	Qty	Description
Lifting Pressure	2	400 bar measuring range
Tilting Pressure	2	400 bar measuring range
Boom Angle	1	180 °measuring range
Bellcrank Angle	1	180 °measuring range

TABLE 5.1: List of sensors for development testing

Table 5.1 lists all the sensors used on the development prototype along with brief descriptions of their functions and ranges. The bellcrank and boom angle sensors are installed in order to compute the implement geometric configuration: starting from the angles, the LABVIEW code can compute the lifting and tilting cylinder extensions L_{1ex} and L_{2ex}.
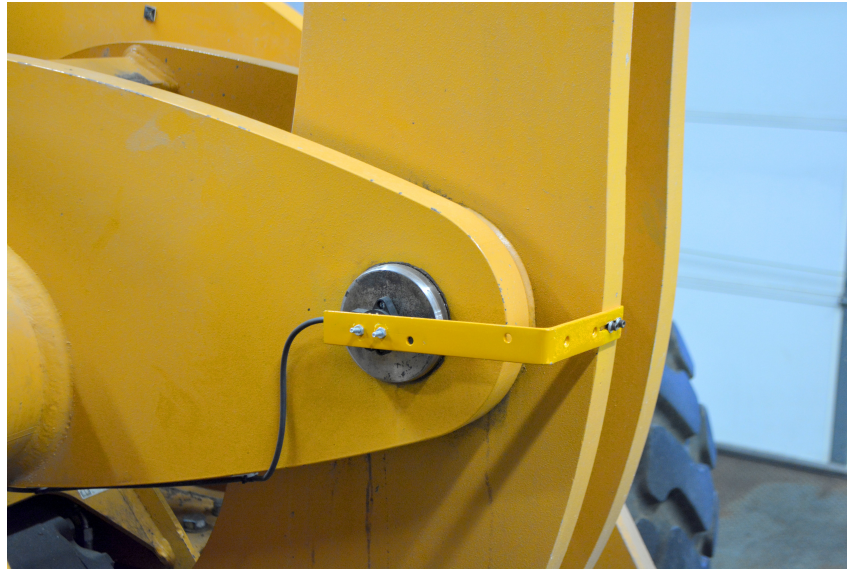
FIGURE 5.7: Bellcrank angle sensor

A direct installation of the bucket angle was not possible due to the heavy cycles performed by wheel loaders: if installed directly on the bucket, the sensor would have been victim of early wearing that most likely would have brought a premature failure. That is the main reason behind the installation of a sensor measuring the bellcrank angle (Fig. 5.7), and indirectly the bucket one. The boom angle, being the absolute angle between hinge O and H along horizontal axis x, is installed directly on the chassis-boom attachment O, as shown in Fig. 5.8:

FIGURE 5.8: Bellcrank angle sensor

Both of the angle sensors have been calibrated with high accuracy: by measuring manually the cylinder extensions, a fitting curve was generated through the use of the analytical model, outputting a boom and bucket angle values for every lifting and tilting cylinders extension. Hence, the voltage read via the LABVIEW code has been converted to degrees throughout the fitting curve.
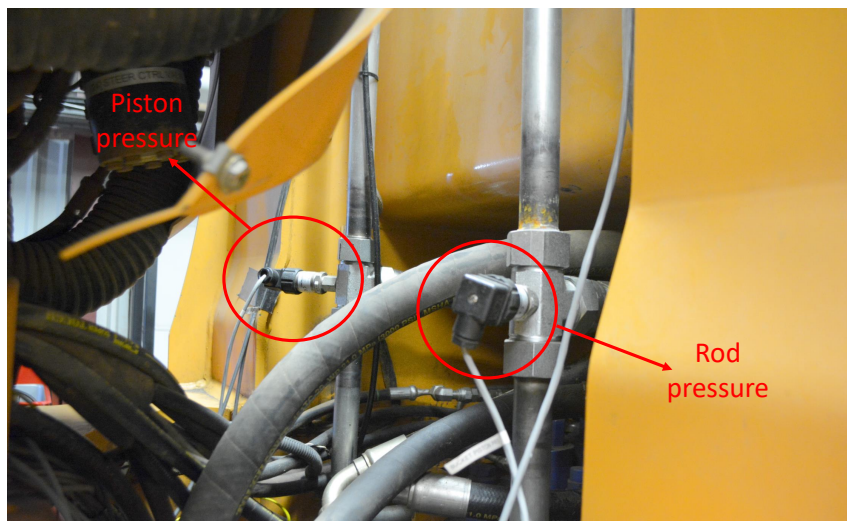
FIGURE 5.9: Tilting rod and piston pressure sensors

Easier from a reasoning point of view was the installation of the pressure sensors since the only issue was actually to find a feasible spot in the pipe bringing the actuating pressure for the installation of the sensors on both the tilting and lifting lines. As shown in Fig. 5.9, the piston and rod pressure sensors have been installed through the addition of a T connection on the driving lines. Same reasoning is valid for the lifting pressure sensors,

as shown in Fig. 5.10:
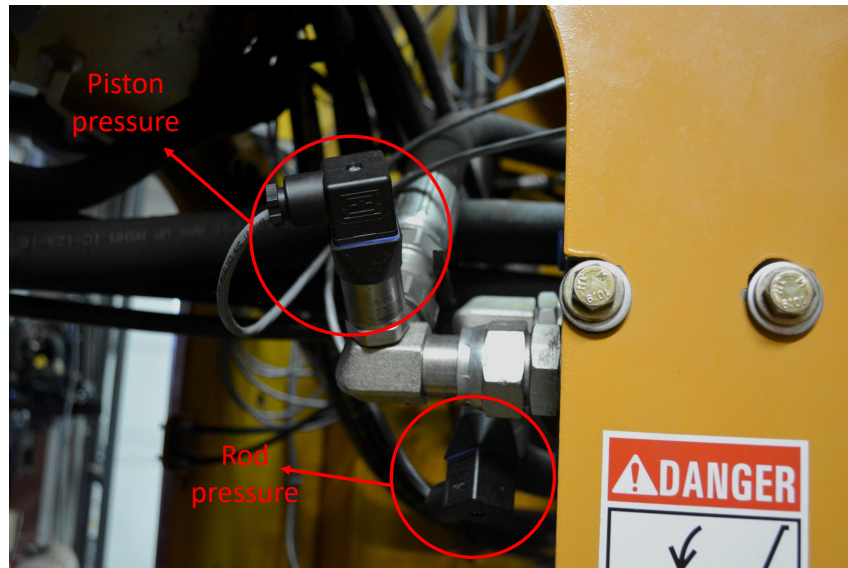
FIGURE 5.10: Lifting rod and piston pressure sensors

The calibration of the pressure sensors was easier since a normalization of minimum and maximum voltage range with respect to minimum and maximum bar output pressure was needed. Fig. 5.11 shows all of the instrumentation for the reference vehicle system, along with the approximate location of each sensor.
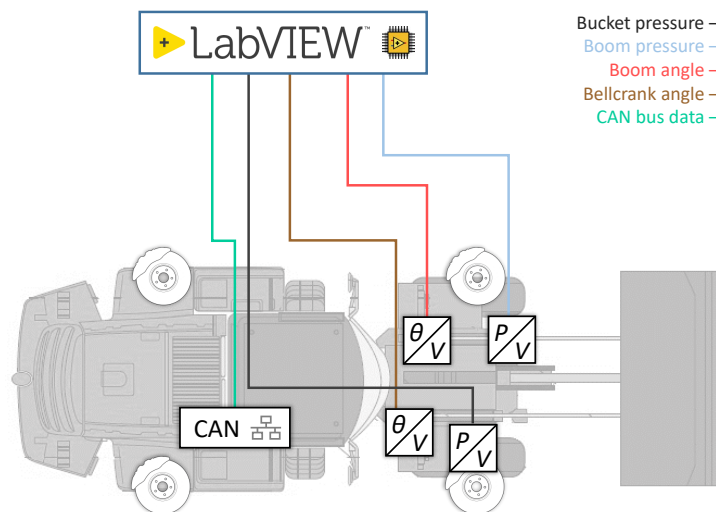
FIGURE 5.11: Sensors overview on the machine

5.3 Model Validation

Once all the sensors are installed, calibrated and the vehicle setup is ready, the first experimental comparison can be done. This section goal aims to validating the system seen in Fig. 3.2 at page 10: starting from the geometric configuration of the implement, tilting and lifting pressures are sensed through the LABVIEW code in order to compute their respective forces. All the data coming from the test is stored into Excel files and passed through the usage of a MATLAB function to its workspace:

$$\texttt{data = xlsread(filename)} \tag{5.4}$$

All the post processing operations, including force computations starting from the pressures, comparisons and plots are therefore performed into the MATLAB environment. The stored values coming from the sensors are:

- Cylinder extensions L_{1ex} and L_{2ex} $\longrightarrow$ the code developed for the inverse procedure is able to compute the cylinders extensions depending on the boom and bucket angle, due to their reciprocity and recalling equations 3.2 and 3.4, we have:

$$L_{1ex} = f(\theta_{boom}) \tag{5.5}$$
$$L_{2ex} = f(\theta_{boom}, \theta_{bkt}) \tag{5.6}$$

  Collecting these values allow a easier post processing operation since the function 5.3 can be called n times, being n the test vector length.

- Hydraulic actuator pressures p_{rod} and p_{piston} $\longrightarrow$ through the use of function 5.7 developed in MATLAB, it is possible, by knowing the annulus and piston surfaces, computing the cylinder force simply with an internal force balance, as shown in Fig. 5.12:

$$F_{cyl} = \texttt{pressure2force}\left(p_{piston}, p_{rod}\right) \tag{5.7}$$

FIGURE 5.12: Cylinder internal force balance

Therefore, the cylinder force is computed as:

$$F_{cyl} = p_{pis} A_{pis} - p_{rod} A_{an} \quad \text{where} \quad A_{an} = A_{pis} - A_{rod} \tag{5.8}$$

The LABVIEW code runs with a sampling frequency of $\approx 20 H_z$, so for 10 seconds of test, 200 element vectors are generated.
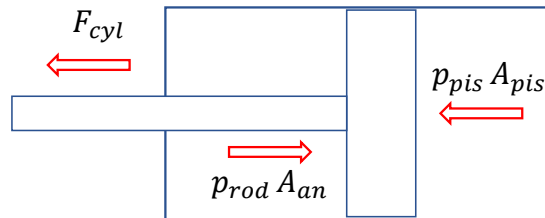
5.3.1 Test Description

The tests performed for the model validation are in steady state operations since the output coming from the MATLAB model is a value that is computed just considering the implement location and the components respective weights (no movement and no inertial terms). Therefore, for both the lifting and tilting force validation, a complete cycle is performed (L_1 and L_2 are respectively extracted from null to maximum stroke) as follows: the not reference cylinder, being the tilting for the lifting phase and the lifting for the tilting one, is kept fixed to an arbitrary displacement. The operational cylinder is extracted ≈ 10 cm at a time in which, for every small extraction, when the implement is not moving (steady state), data coming from the sensors is recorded and stored. Doing so, we achieve comparable data that can be used to validate the simulated models.

5.3.2 Results Comparison

The first force to be analyzed is the lifting one, considered at just one of the two cylinders, since the sensor were mounted singularly on only one of them. In the following test performed, the tilting cylinder extension has been set to 0.37 m, value that could have been computed thanks to the LABVIEW code. After that, the lifting cylinder has been extended from null to maximum stroke, as shown in Fig. 5.13 where in yellow we can see the numerical model trend, in red the kinematic simulated one, in blue a continuous lifting cycle (no steady state measurement performed here, just boom completely raised with constant velocity) and in green the steady state samples taken during a lifting cycle. First of all, it is noticeable how the measured data plots are shifted with respect to the y axis and start at $L_{1ex} \cong 5$ cm. This is because the location in which the test has taken place was with a even ground and therefore the boom minimum extension was reaching ≈ 0.05 m because of the bucket bottom plate touching the ground.

Besides, it is worth of mention that the continuous lifting plot has been recored just to have an idea of how the frictional and inertial effects contribute on the force demanded by the hydraulic actuator. That being said, we clearly can see from the plot how, for the
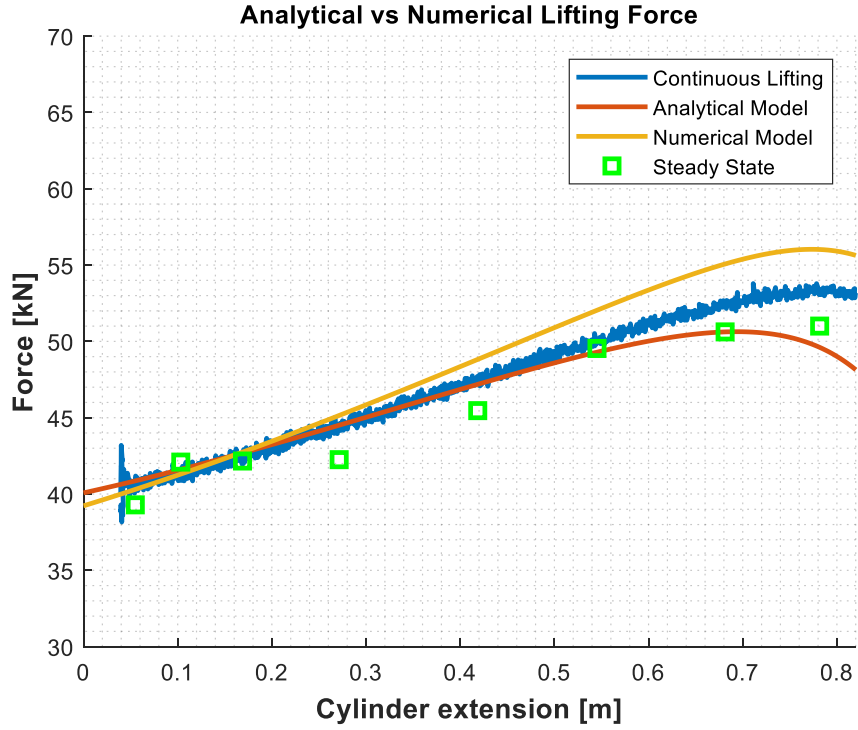
FIGURE 5.13: Experimental lifting force comparison on one actuator

available cylinder extension range, the measured data follows the expected trend given by the simulated models. Besides, it is evident how all the four plots follow an essentially identical trend for the first half of the extension. The second half of the plot shows how the measured steady state data aligns its trend close to the analytical model instead of the numerical model that here should be the one closest to the real behavior of the machine. Anyways, the difference between steady state measured data and numerical model varies in a $3 \div 5$ kN range, which could be a reasonably small number since we are managing a 16 tons machine and the forces acting on the system are always very high in magnitude, even for steady state situations where the machine is not moving at all. Moreover, during the experimental tests performed, the bucket was missing the cutting edge-on for wear prevention so, the bucket weight inputted into the code was not perfect. This could have easily led to a reduction of the lifting force needed. Besides, sensor and/or measuring errors could have effected the result too but again, all the plots follow a very similar trend with low offset between them so the result obtained can be assumed acceptable.

A more satisfying outcome is achieved on the tilting force measurements as shown in Fig. 5.14 where a complete cycle is performed keeping a fixed $L_{1ex} \cong 0.44$ m.

First of all we can notice how here, with respect to Fig. 5.13, both the steady state and the continuous measurements start at null cylinder extension. All the plots follow a pretty neat trend during all the tilting phase. In the first half of the test, being from $L_{2ex} = 0$ to $L_{2ex} \cong 0.3$ m, we obtain the maximum difference between the four plots: the steady state
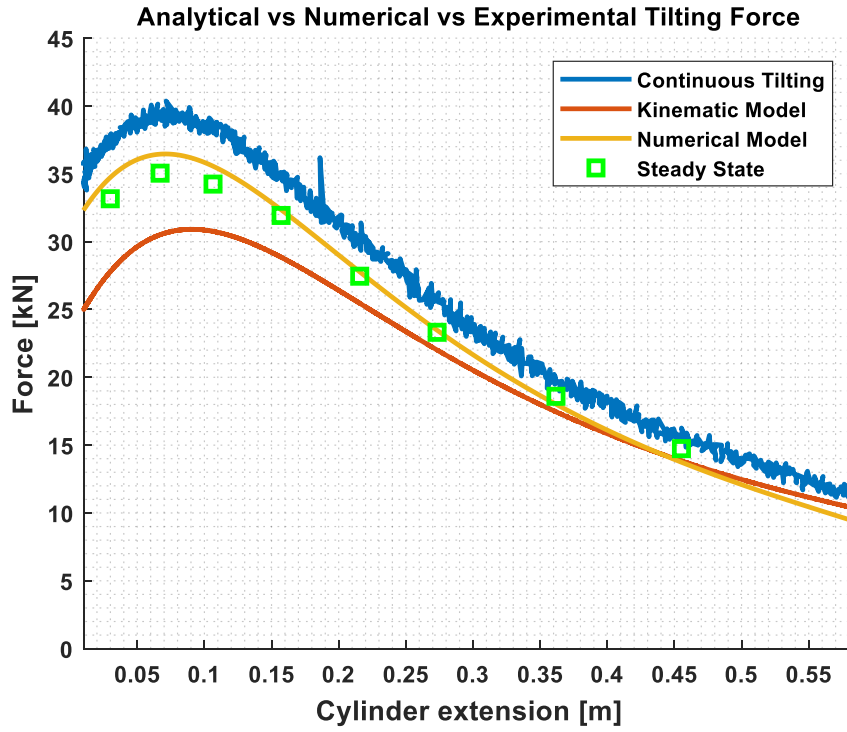
FIGURE 5.14: Experimental tilting force comparison

measurements are anyways very close to the numerical model, as expected, even during this first crucial part of the test. The analytical model is the one obtaining the lowest demanded force. As soon as we move into the second half of the plot, we can clearly see how all the four plots converge to almost the same values, decreasing distinctly the difference between them. It is correct to state here that the result obtained for the tilting force F_{CD} is more than adequate. Besides, an interesting behavior is the one brought by the continuous tilting where we witness always a higher force demanded by the actuator: this could be probably due to the frictional effects acting on the cylinder, here more visible with respect to the lifting ones.

The overall result of the model validation is positive since a very similar trend of the expected curves has been achieved for both the lifting and tilting phase. The data values computed are also very close to either the numerical or the analytical model so, by using the models developed, we can now move forward and try to validate the inverse procedure computing the external forces acting on the bucket.

5.4 External Force Estimate

Having validated the analytical model, it is possible now to make one step forward and validate the system shown in Fig. 3.17 at page 23, being the inverse procedure of the

analytical model: starting from the implement geometric configuration, measuring θ_{boom} and θ_{bkt}, and the hydraulic actuator pressures p_{rod} and p_{piston}, the system is able to compute if any external disturbance force is acting on the bucket center of gravity and to get its magnitude along the x and z axes.

5.4.1 Test Description

The field tests were run into a Purdue University ABE (Agricultural and Biological Engineering) department complex. The availability of a heavy off-road machine scale led to appropriate reference measurements. The external force validation is made up of a four point test:

- Completely empty bucket

- Medium-low load

- Medium-high

- Completely full bucket (Fig. 5.15)

FIGURE 5.15: Field tests at the Purdue ABE complex with reference machine

For every of the four loading situation, the vehicle was brought to a proper scale, having a maximum error of $\pm \approx 60$ lbs and being located around 500 m from the digging pile, to get the reference payload quantity. Thus, for every test set, the current load was measured firstly with the model developed, secondly with he state of the art present on the machine,

This tool gets an estimate of the payload on the bucket by lifting the boom from minimum to almost maximum extension and depending on parameters as boom pressures, lifting velocity and engine rpm. Finally the vehicle was brought to the scale in order to get the proper measurement. Therefore, some factors have to be taken into account as gas consumed during the way to the scale, possible small dirt losses during the state of the art measurements and during driving operations. The data recored was thereafter processed and analyzed at the Maha Fluid Power Research Center by converting all the recorded measurements into the same SI (kN) and by creating a table expressing the respective errors (of the state of the art and the model) with respect to the scale.

5.4.2 Results Comparison

Table 5.2 shows the data recorded for the four tests: it is clear that the scale is weighting the whole machine whilst the state of the art and the model measurements are strictly related to just the load on the bucket, as shown in Fig. 5.16:
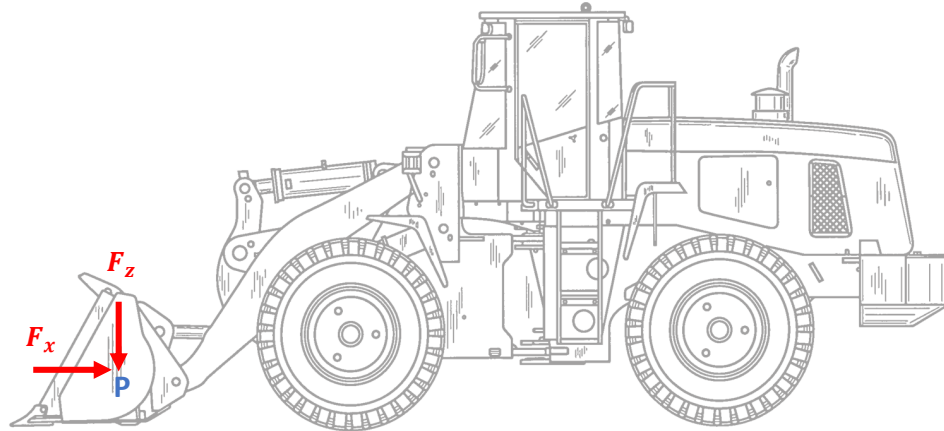
FIGURE 5.16: F_z and F_x forces acting on the bucket

Test	Scale [lbs]	State of the art [lbs]	Model [kN]
Empty bucket	32320	160	0.669
Medium-low	35300	3020	12.37
Medium-high	39020	6630	30.32
Full bucket	42280	9840	44.9

TABLE 5.2: Four point test raw results

Some data processing was necessary in order to have comparable data: firstly, the machine weight, given by the empty bucket measurement of the scale, has been subtracted to all

the scale measurements in order to get purely the payload on the bucket. Moreover, for both the state of the art and the scale the conversion from lbs to kN has been performed as follows:

$$\vec{W_{kN}} = 0.4536 \cdot \vec{W_{lbs}} \cdot \vec{g} \quad [\text{kN}] \tag{5.9}$$

where $\vec{g}$ is the gravitational acceleration and 0.4536 is the lbs to kg conversion ratio. Performing this operation we obtain Table 5.3:

Test	Scale [kN]	State of the art [kN]		Model [kN]	
Empty bucket	0	0.712		0.669	
Medium-low load	13.26	13.44	$\mathcal{E}= 1.34\%$	13.55	$\mathcal{E}= 2.19\%$
Medium-high load	29.81	29.50	$\mathcal{E}= -1.04\%$	30.32	$\mathcal{E}= 1.70\%$
Full bucket	43.946	43.785	$\mathcal{E}= -1.20\%$	44.32	$\mathcal{E}= 1.31\%$

TABLE 5.3: Four point test post processed results

where all the data is expressed in kN. First of all, it is noticeable how a maximum error of $\approx 1.3\%$ and $\approx 2.2\%$ is achieved for state of the art and model, respectively. Besides, we can clearly see how the model error decreases with an increase of the payload: this more significant error at low payloads can be explained by small oscillations of the sensor pressures for lower payloads. The overall result for the payload F_z is quite good for the developed model: a maximum difference of $\approx 0.9\%$ is obtained with respect to the state of the art. In addition, we have to consider that the measurements achieved from the state of the art require a boom raising in order to have an output result while the ones obtained by the model jut require the wheel loader bucket to exit from the pile. This is a crucial aspect if we think about efficiency terms: state laws constrain the semi-trucks carrying dirt to maximum predefined loads in order to prevent premature road wearing. Thus, if a wheel loader is loading a semi-truck and gets a total weight exceeding the allowed one, it will have to drop some dirt before moving to the next truck. It is clear how, with the model developed, the driver operator can immediately recognize an exceeding load as soon as he/she finishes the loading cycle and drop almost simultaneously some dirt. By relying on the state of the art instead, a complete boom raised would be needed and, in case of exceeding weight, the operator should have to drop some dirt, lower the boom and raise it again in order to achieve a new measurement. Therefore it is pretty evident how, spanning the operations for work operating hours and days, the model payload computation could bring to a solid efficiency improvement.

As shown in Fig. 5.16, our external force computation does not only apply for the payload but, always with respect to the bucket center of gravity, calculates an estimate of the horizontal force F_x acting on it. Nevertheless, the external force validation has brought some issues in terms of criteria. Since no horizontal scale was available, no proper measurement

reference was possible. For the four points test of 5.3, an almost null constant horizontal force was obtained, as shown in table 5.4:

Test	F_z [kN]	F_x [kN]
Empty bucket	0.669	0.55
Medium-low load	12.37	0.359
Medium-high load	30.32	0.437
Full bucket	44.9	0.14

TABLE 5.4: Four point test for horizontal and vertical estimate

Therefore, we can state that the horizontal force estimate validation is given by the vertical one since erroneous horizontal estimate values would have brought to wrong payload computations. However, an approximate trend result of the horizontal estimate was computed with a few in-lab tests as follows. The test rig shown in Fig. 5.17 has been built for an on-going research project aiming in developing an electro-hydraulic traction control system for the reference machine.

FIGURE 5.17: Horizontal force F_x test rig

The tractor wheels fixed to the ground are supposed to simulate the behaviour of a pile giving a purely horizontal counterbalance force during digging operations, as shown in Fig. 5.18 where the force F_p [N] is the horizontal force given by the wheels, modelled as a damper-spring parallel connection and h_p [m] is the height at which F_p is applied. It is also noticeable the presence of four plates attached to the concrete: their purpose was to allow the wheels slip after achieving a certain maximum horizontal force by the tires (the whole set-up was built for traction control purposes).
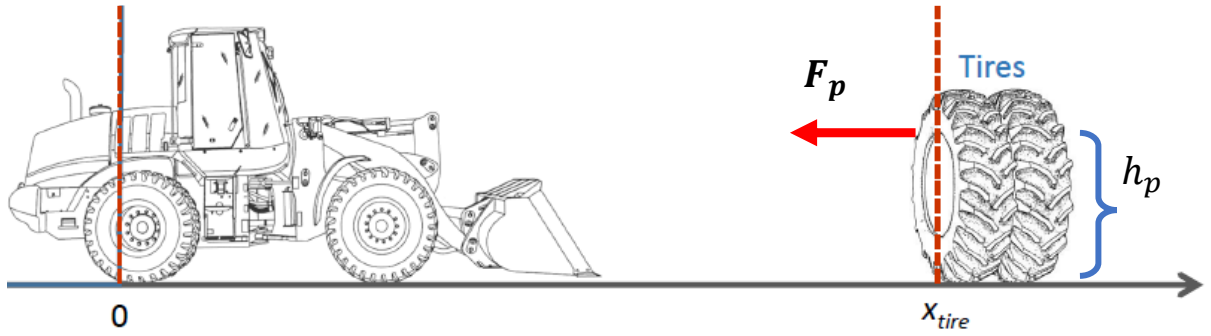
FIGURE 5.18: Reaction force given by the wheels simulating a pile

So, in order to perform the tests, another modification to the reference machine was needed. A steel plate was mounted on the bucket edge-on attachments vertically with respect to the horizontal plane, as shown in Fig. 5.19 so that an homogeneous pushing force could be achieved. The boom and bucket angles for all the tests were set so that the plate was fully pushing into the wheel system.

FIGURE 5.19: Reference machine with steel plate on

Therefore, a few tests were run as follows: the acquisition system was turned on with the vehicle approaching the wheels with a predefined and fixed boom and bucket angle. Thus, the wheel loader was reaching the wheels at starting pushing against them with, clearly, a linear velocity reduction due to the force coming from the wheels. A maximum pushing force was achieved before the tires slip and after that, the throttle was released in order

to decrease the horizontal pushing force. The pushing/releasing procedure was performed three times. The Fig. 5.20 shows the results achieved from the test:
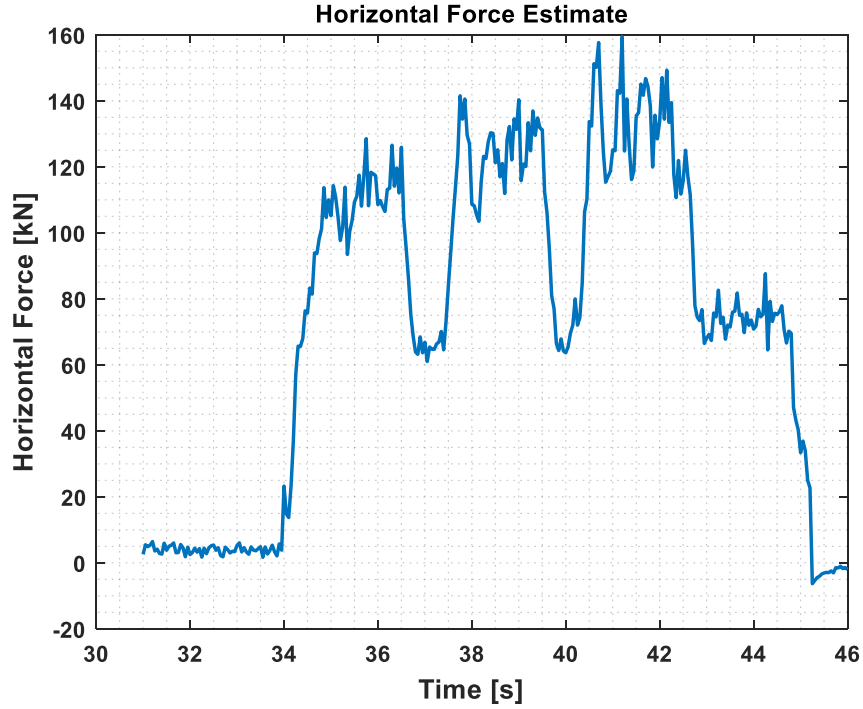
FIGURE 5.20: Horizontal force F_x for in-lab test

First of all, we can notice how the trend behaviour reflects the expected one: the horizontal force estimate starts and ends with an almost null value, meaning when the vehicle is not touching the wheels system and is just approaching or receding it. That being said, we can clearly see how we achieve three similar peaks that are due to the three push and release phases. The main problem here with the validation, as stated before, is that we do not have any reference pushing force magnitude with can compare our data with. So we will assume that, besides the coherent trend achieved, we are also getting a correct magnitude value since the payload measurements were very accurate. Besides, without going into much detail, the model was used also for the traction control project and very relevant results were obtained for non linear-controllers when the horizontal pushing force was computed with the model.

Chapter 6

Work Pile Simulation Model

This chapter aims in explaining the old pile model deficits and therefore the need of a new study for the interaction forces acting during a digging cycle. The first subsection will introduce the current pile model whilst the second one introduces the work done for a better and more complex one. It is worth of mention that, the current approach found before my work was purely designed and used for traction control simulations. Therefore, even if very simplified, this model had brought solid results for the needed and performed simulations.

6.1   Current Approach

The current pile model present in the vehicle dynamic system is the one expressed in Fig. 6.1 where the reaction force given by the pile F_P [N] is completely horizontal (along x axis) and acting at a certain predefined high h_p [m], $2F_{N1}$ $2F_{x1}$ [N] and $2F_{N2}$ $2F_{x2}$ [N] are the normal and axial forces acting at the front and rear wheels, respectively, and they were needed for the pushing force given by the machine computation; mg [N] represents the vehicle weight whereas ma_x [N] its inertial term.
The pile force is modelled as a parallel connection of spring and damper working only in one direction (positive x), being it:

$$F_p = \begin{cases} k_p x_p + \beta_p \dot{x}_p, & \text{if} \quad x_p \geq 0 \text{ and } \dot{x}_p \geq 0 \\ 0, & \text{else} \end{cases} \tag{6.1}$$

where k_p [N/m] and β_p [Ns/m] represent the stiffness and damping coefficients related to the resistive force of the pile. This model clearly shows a lack of accuracy since many
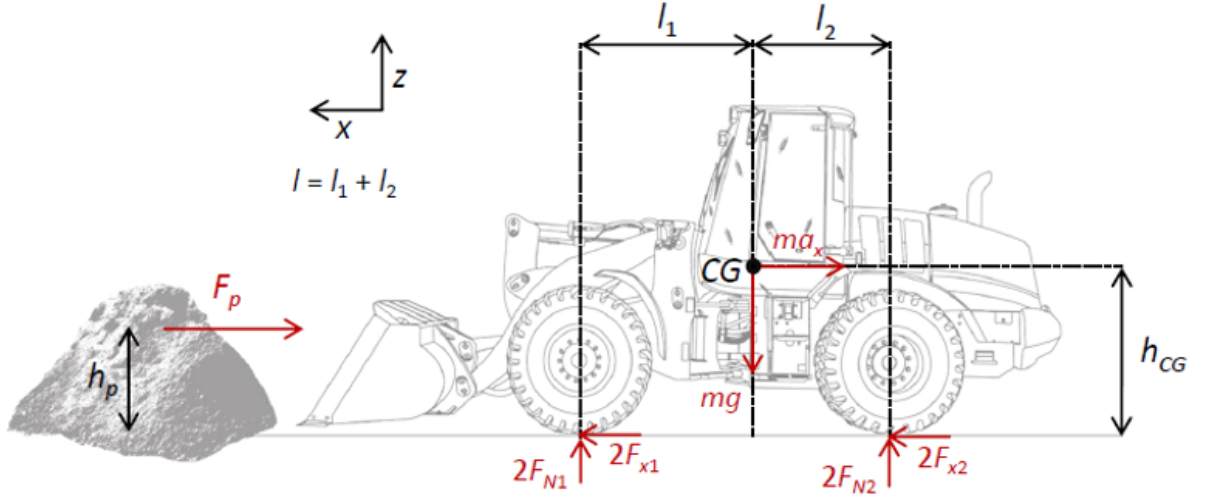
FIGURE 6.1: Reaction force of the pile model

terms (hereby some of them are cited) are neglected: frictional forces, any force exchanged between bucket and pile that is not along the x axis, moments along the z axis, etc. As cited in [1], [2], [3] and other papers/books, a general digging cycle of a wheel loader can be divided in three simplified phases, as shown in Fig 6.2:

FIGURE 6.2: The three phases of a digging cycle

- **Crowding (phase 1)** $\longrightarrow$ the bucket penetrates inside the pile with a null or negligible angle with respect to the ground through wheel revolution. This one lasts until the human operator feels an exceeding resistive force: once a critical digging depth or forward speed is reached, the transition to phase 2 is triggered.

- **Bucket filling (phase 2)** $\longrightarrow$ the bucket moves inside the pile following a line or curve path (usually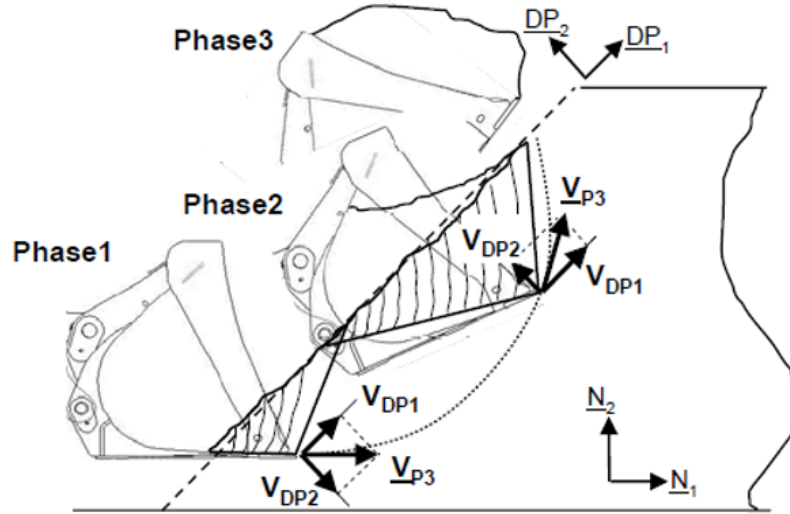 tending to minimize the energy consumption) with a fixed or varying tilting angle. The trigger between phase 1 and 2 can be modeled as the actuation of either the lifting and/or tilting cylinders by the hand of a human operator. When the bucket is completely filled phase 3 is active.

- **Rollback (phase 3)** $\longrightarrow$ tilt cylinder actuated until the fully rolled position is reached. Consequently (or simultaneously) the lift cylinders are actuated bringing the overall behavior almost to a straight vertical movement exiting the pile.

Hence, taking into account this phase division, it is clear that the force model expressed by Fig. 6.1 neglects completely phases 2 and 3 (and their respective non-horizontal forces terms). Moreover, it is not granted that the horizontal reactive force of phase 1 grows linearly with displacement and velocity so, a priori, we cannot assume accurate and correct a model designed through purely just spring and damper. Nevertheless, for the initial purpose of the system, this was an acceptable simplified assumption that brought to satisfying in-lab test results on the EH traction control since the actual pile, unavailable at the Maha Fluid Power Research Center lab, was substituted with a set of tires perpendicular to the ground, as shown in Fig 6.3.
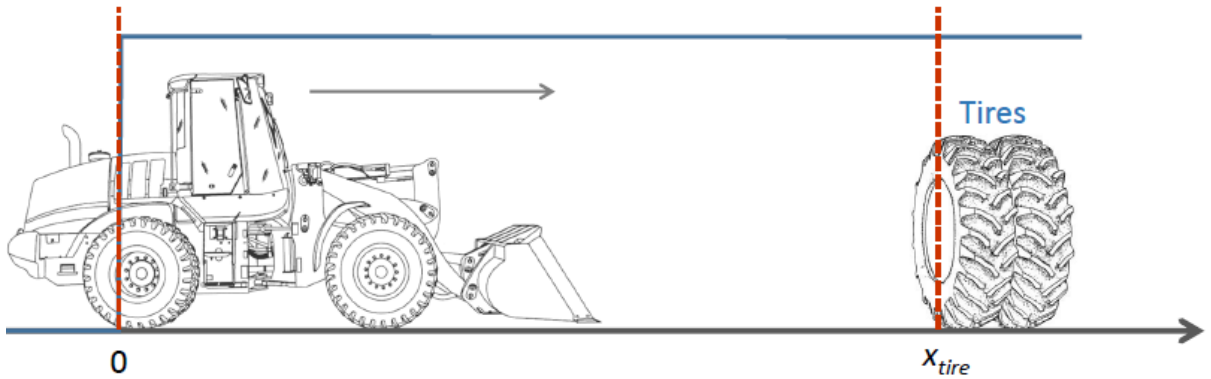

FIGURE 6.3: Experimental setup for the lab tests run for the traction control

In conclusion, the investigation of a new pile model that took into consideration all of these aforementioned neglected terms was necessary.

6.2 Multi-Component Digging Force Analysis

The investigation presented in this section presents a new formulation of a more complex pile model. This one is coded and implemented into a MATLAB/Simulink software environment and moreover a simple simulation, in order to show how the forces change their contribution during a scooping cycle, is run and discussed.

6.2.1 Model Composition

The model presents five forces that are continuously inter-exchanged between pile and bucket. These five forces are not a novel concept in literature since they are cited, used or taken into account in many works and papers as in [1] and [3]. The overall view of the force-system is shown beneath in Fig 6.4:
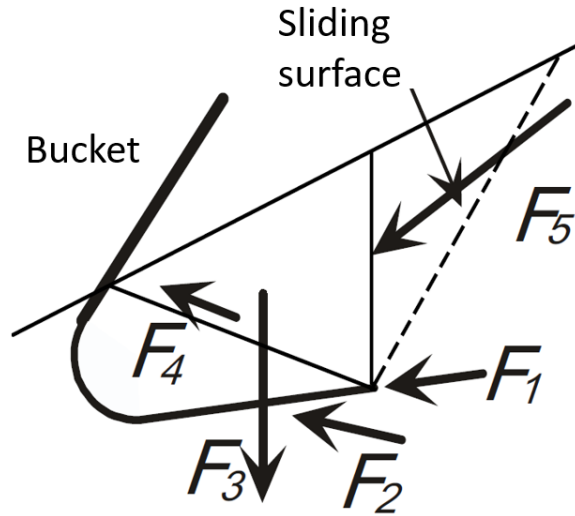
FIGURE 6.4: Bucket snapshot showing the 5 forces acting on it

where the forces are generated by the pile during a digging cycle. Hence, the wheel loader will have to provide proper counter reacting force in order to move boom and bucket through the dirt. A useful screen of the system geometry properties proposed by [1] is illustrated in Fig 6.5 where β [°] is the pile angle with respect to ground (considering a linear increment of its high), σ [°] is the angle between the bucket plate and the dirt inside it, H [m] is the digging depth measured from the bucket tip to the pile surface, κ [°] is the motion direction angle and finally ζ [°], angle between ground and bucket tip. Thanks to [4] and [5] it is possible to express these five forces as follows:

FIGURE 6.5: Bucket geometric parameters

- **Penetrating force at the bucket tip F1:**

$$F1 = K cos(\kappa) \gamma H S g \tag{6.2}$$

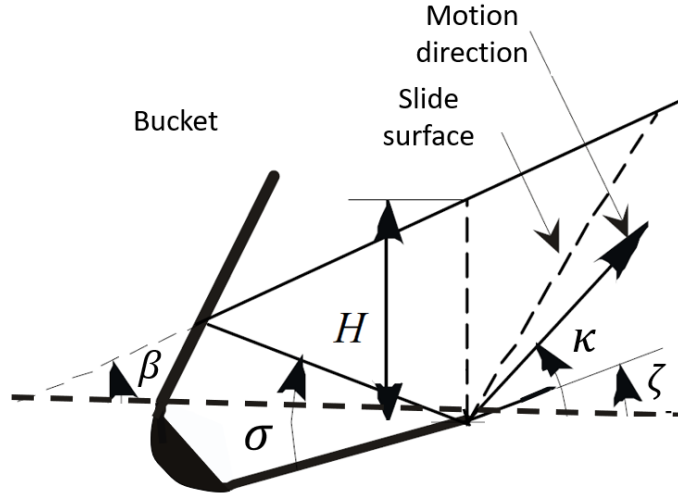where H [m] is the bucket depth with respect to the pile surface, K [/] is the coefficient related to the penetration resistance for each material, γ $[\frac{kg}{m^3}]$ is the dirt specific gravity, $g[\frac{m}{s^2}]$ is the gravitation acceleration and $S[m^2]$ is the cross sectional area of the bucket's tip. However, a problem raises immediately: in fact, with this empirical formula, the uncertainty related to the parameter K is so high that finding a proper range of K values for the various configurations is not possible. For this reason, the sinkage empirical formula in [6] is introduced:

$$p = \left(\frac{k_c}{b} + k_\phi\right) z^n \tag{6.3}$$

where p [Pa] is the pressure acting on the bucket's tip surface, n [/] is the exponent of deformation, z [m] is the sinkage depth, b [m] is the width of penetrating surface and $k_c[\frac{kN}{m^2}]$ and $k_\phi[\frac{kN}{m^2}]$ are the cohesive and frictional moduli of deformation, respectively. By multiplying the load pressure for the cross sectional area S obtained by equation 6.3, we can obtain F1. Bekket's empirical formula is preferred due to the higher knowledge behind the factors composing it. Clear useful tables are exploited for the moduli of deformation, the exponent of deformation is almost always assumed unitary and the width of penetrating surface, playing a critical role in the formula, has been found to be optimal if set to half the cutting blade thickness.

- **Resistance force at the bottom of the bucket F2:** it appears just when $\kappa > \zeta$. However, such configuration is normally not reached at practice operation. Anyhow,

even if sometimes present, this specific force would actually help the bucket rotation, since it contributes by giving a positive momentum around the bucket rotation motion. A lot of on-going studies are aiming in finding an empirical formula to describe F2. In any matter, this force will be neglected in our work.

- **Weight load of the material inside the bucket F3:**

$$F3 = M(t)g \tag{6.4}$$

where $M(t)$ [kg] is the load, varying in time, inside the bucket and $g[\frac{m}{s^2}]$ is the gravitational acceleration. The payload mass is highlighted to be time dependent since we wanted to avoid any assumption or misunderstanding of fixed load during scooping operations. It is worth of mention that all these five forces composing the model are clearly time dependent since there is a strict correlation with the bucket motion inside the pile.

- **Frictional force between bucket and dirt inside it F4:**

$$F4 = \mu\, F3\, cos(\zeta) + \mu\, F5\, cos(\phi - \zeta) \quad \text{if} \quad \dot{x_{rel}} > 0 \tag{6.5}$$

where ϕ [°] is the soil internal friction angle characteristic of the particular dirt and condition (dry sand, wet sand, gravel, rocks, etc.) and μ [/] is the friction coefficient between the bucket plate and the dirt inside the bucket. The relative velocity between materials and bucket's plate $\dot{x_{rel}}$ impose the frictional force presence (if the bucket stays still, clearly no frictional effect is witnessed).

- **Force required to move the material in front of the bucket F5:**

$$F5 = P_P A_{bkt} = \frac{\gamma H^2}{2} \frac{1}{sin^2(\beta)sin(\beta - \delta)} \frac{sin^2(\phi + \beta)}{\left[1 + \sqrt{\frac{sin(\phi+\delta)sin(\phi-\beta)}{sin(\beta-\delta)sin(2\beta)}}\right]^2} A_{bkt} \tag{6.6}$$

where $\gamma[\frac{kg}{m^3}]$ is the material density, $A_{bkt}[m^2]$ is the area related to the virtual plane, H [m] is the sinkage depth, β [°] is the pile inclination, ϕ [°] is the internal friction angle of the soil and δ [°] is the angle related to the shear stress. In phase 2, which is the most critical, the material inside the bucket generates a fictitious face, called virtual plane, pushing the pile. F5 is hence computed using the passive soil pressure formulated by Coulomb, which can be applied with consideration to the virtual plane as the wall. On the virtual plane, no shear stress is supposed to be appeared. Hence F5 is obtained by equation 6.6 with $\delta = 0$. The Coulomb pressure times the surface of the virtual wall, considered as the perpendicular plane covering the bucket face, gives the force F5.

6.2.2 Model Implementation

The following subsection illustrates how the five force system seen before has been developed into MATLAB/Simulink environment.
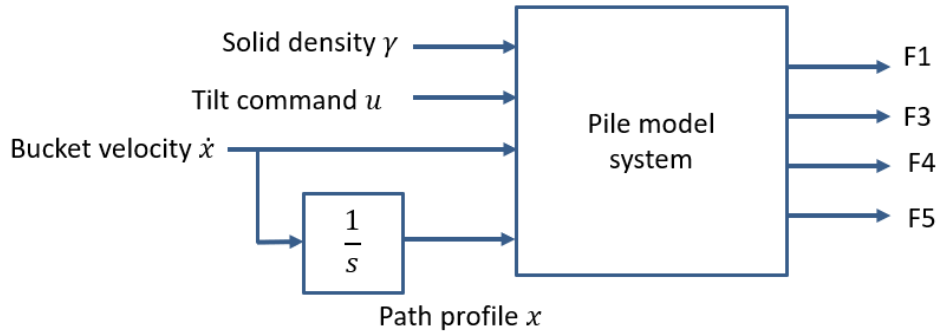

FIGURE 6.6: Pile model system with its inputs and outputs references

The overall system overview is shown in Fig 6.6 where the system inputs are the material solid density $\gamma[\frac{kg}{m^3}]$, the tilting command u [°] (usually provided by the operator), the bucket velocity $\dot{x}[\frac{m}{s}]$ in which it is moved inside the pile and its relative path profile $x[m]$. The outputs are clearly the four forces seen in 6.2.1, keeping in mind that the force F2 acting underneath the bucket is here neglected.

6.2.3 Simulation Results

As stated before, a simple simulation in order to see and understand how the forces behave during a complete digging cycle is run. Table 6.1 illustrates all the parameters needed to simulate the pile model. Some of the quantities seen in the section exploring the force formulations are directly computed in the Simulink sub-blocks.
A perfect linear pile is here assumed with a certain height h_p and a arbitrary depth l_p. The trajectory path performed by the bucket inside it is a parabolic trend with a constant relative velocity v_{rel} (and therefore, null acceleration $a_{rel} = 0$). Bucket parameters as cutting edge and width are directly taken from the reference machine data-sheet (remembering that from Bekket's formula, the ideal width of penetrating surface is given by the half of the cutting edge). The dirt is here assumed to be dry sand (any other bulk material could have been chosen) with its relative properties as solid density, internal friction angle and the consequent friction coefficient between it and the bucket plate. Frictional and cohesive moduli of deformation complete the parameters needed for Bekket's pressure formulation. It is worth of mention that, in order to enter in the metric system, the solid density had

Wheel Loader relative speed	$v_{rel} = 0.25$ [m/s] = constant
Pile height	$h_p = 3$ [m]
Penetration depth	$l_p = 1.5$ [m]
Bucket width	$bkt_{width} = 2.7$ [m]
Bucket cutting edge	b = 0.03 [m]
Friction coefficient between bucket and dirt	$\mu_{bkt} = 0.28$ [/]
Solid density	$\rho = 2.67 \left[\frac{gr}{cm^3}\right]$
Soil internal friction angle	$\phi_{soil} = \pi/6$ [rad]
Pile inclination	$\alpha = \tan^{-1}\left(\frac{h_p}{l_p}\right) = 63.44[°]$
Cohesive moduli of deformation	$k_c = 5.27 \left[\frac{kN}{m^2}\right]$
Frictional moduli of deformation	$k_\phi = 1515.04 \left[\frac{kN}{m^2}\right]$
Exponent of deformation	n = 1 [/]

TABLE 6.1: Parameters needed for pile model simulation

to be turned into kilograms and meters, hence:

$$\rho = 2.67\left[\frac{gr}{cm^3}\right] \longleftrightarrow \rho = 2670\left[\frac{kg}{m^3}\right] \tag{6.7}$$

The solver and simulation properties for the Simulink software environment are the following:

$$\begin{cases} \text{Initial and final time} \quad \longrightarrow \quad T_i = 0 \text{ s} \quad T_f = 6 \text{ s} \\ \text{Type: Variable-step with Automatic solver selection} \\ \text{Sampling-step size (fundamental sample time)} \quad \longrightarrow \quad T_s = 1 \text{ ms} \end{cases} \tag{6.8}$$

The sampling time is referred to the frequency with which data is sampled and stored into MATLAB workspace. Therefore the obtained vectors from the simulation will be made up of 1×6000 elements, since the window for the simulation is exactly 6 seconds. The window time is not decided a priori but, depending on the pile, bucket trajectory and relative velocity properties, it may vary. The values assumed here, expressed in table 6.1, were taken and simplified by real-world applications. Anyways, this passage to MATLAB is done in order to perform some post-processing operation, as, for example, simply plotting the desired values. So, the simulation consists in a digging cycle performed by a wheel loader keeping a constant velocity during the whole operation; the path covered my the bucket is a parabolic trend starting from the pile bottom and ended when the bucket exits the pile, ash shown in Fig. 6.7. The bucket profile for the purpose of this simulation is considered to be the trajectory given by just the edge. Besides, as shown
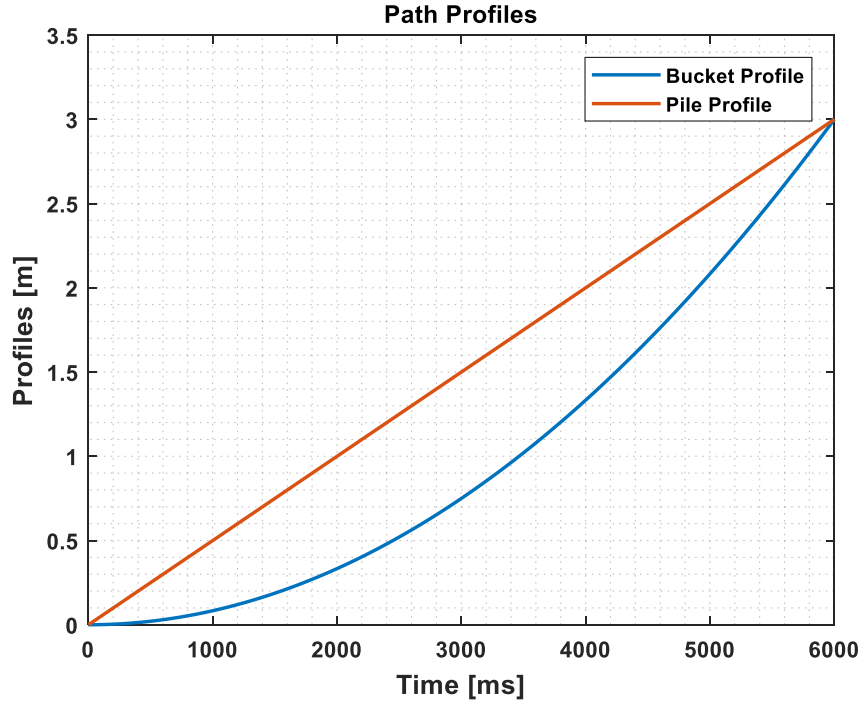
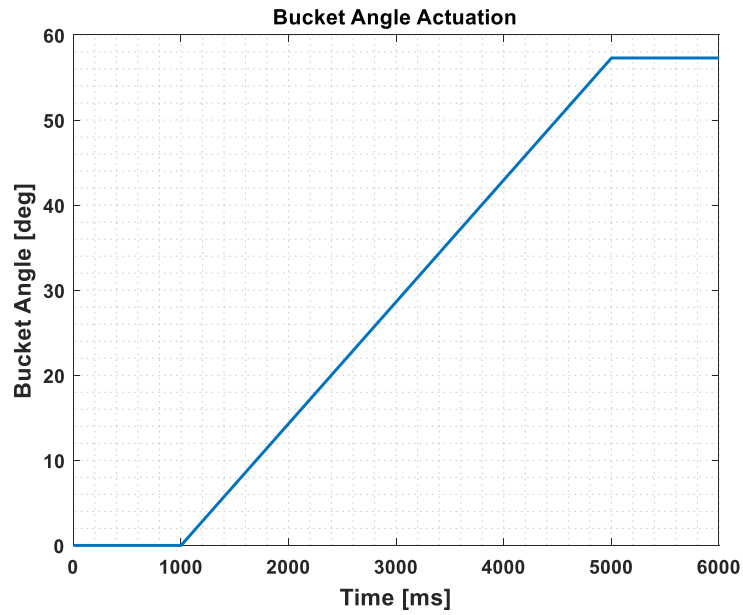FIGURE 6.7: Pile and bucket trajectory profiles over time

in Fig. 6.6, our model gets as input also the tilting command performed by the operator in the vehicle cabin. Again, data recored from real-world applications brought to this simplification: the bucket is tilted from $\theta_{bkt} = 0$ °to $\theta_{bkt} = 1rad \cong 57.3$ °in a linear trend, lasting 4 seconds (Fig. 6.8).

FIGURE 6.8: Tilting command u over time

We can now focus our attention on the forces in play: as seen in equation 6.3, the penetrating force at the bucket tip F1 exponentially (linearly here, due to the unitary value for the exponent of deformation n) depends from the sinkage depth H.
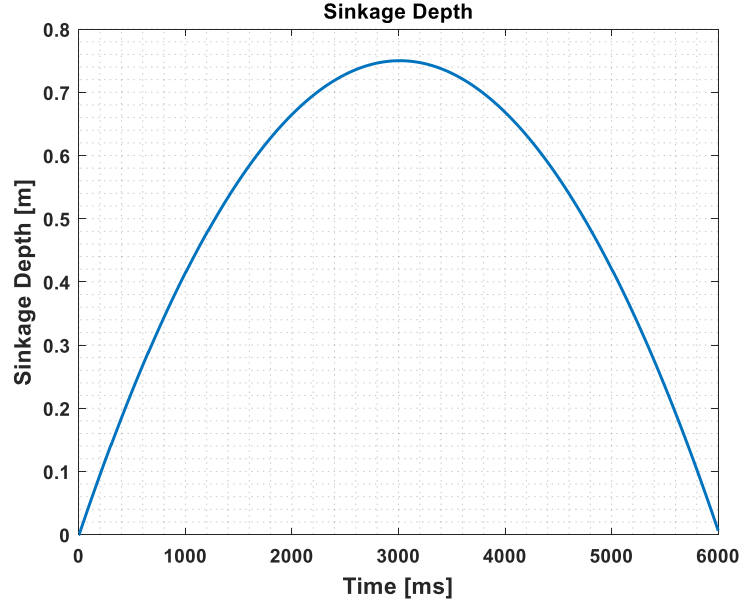

FIGURE 6.9: Sinkage depth trend over time

Therefore, as shown in Fig. 6.9, a maximum value is reached during approximately half simulation, where $H_{max} \cong 0.73$ m. Hence, we expect from F1 a similar trend since the other parameters in the equation stays constant during time. The result is shown in Fig. 6.10(a) whereas in Fig. 6.10(b), F1 trend is given using the empirical formula seen in 6.2.
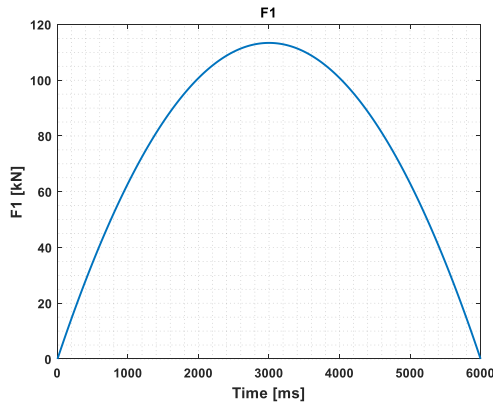
(a) F1 trend over time using Bekket's pressure formula
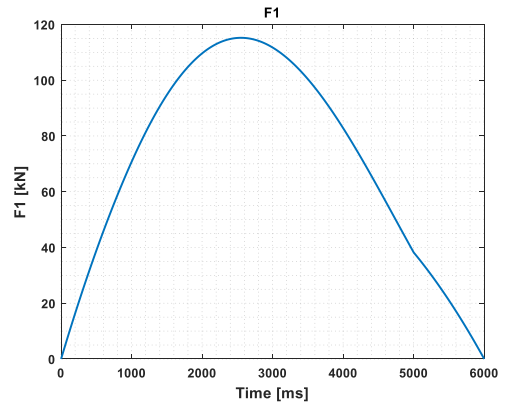
(b) F1 trend over time using the empirical formula

FIGURE 6.10: F1 trends over time

The uncertainty related to parameter K is here avoided since it has been tuned in order to match, in amplitude, the values obtained from Bekker's formulation. We can clearly see how both the plots follow a very similar trend, achieving a peak when H_{max} is reached.

Nevertheless, the empirical formula of 6.2 it has been used here just as double check. It also makes sense that F1 is increasing during the first half of the plot, since during phase 1 its value reaches criticalness. Besides, both the trend goes to zero when the simulation is finished, meaning that there is no resistive force, of course, when the bucket exits the pile. Moreover, the tilting command creates a failure in the resistive force at the bucket tip, therefore, its decrease in the second half of the simulation when the bucket angle has reached a relatively high value that brings a drop for F1 magnitude. Again, we recall the fact here that no accurate verification or validation can be performed here, but just the trend and the magnitude of the forces are investigated (whilst the validation is left as future work). Nevertheless, regarding the payload force F3, a mathematical validation can be performed.
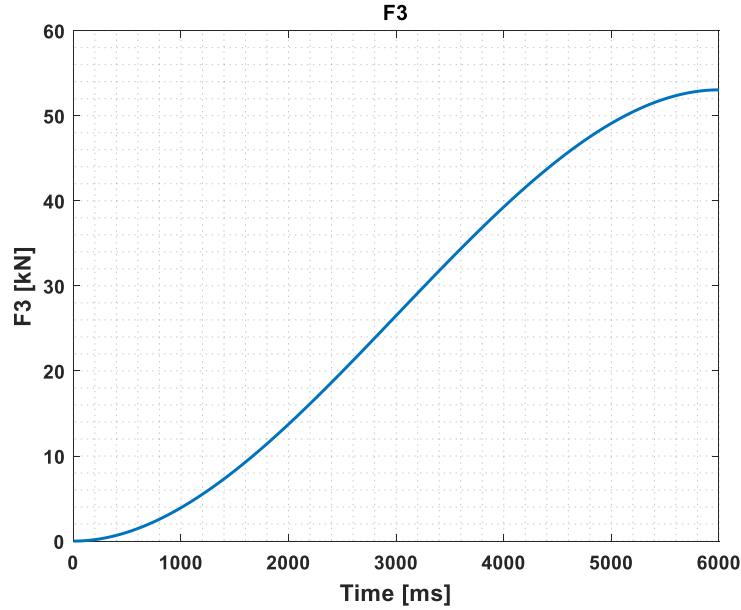
FIGURE 6.11: Payload F3 trend over time

Fig. 6.11 shows the payload trend during the digging operation: as expected we have a monotonic trend increasing over time until it levels out around ≈ 53.04 kN. As stated before, a mathematical verification can be performed for the payload since it can be computed easily by integrating the area between the two trajectories seen in 6.7. Multiplying the area by the bucket width, we obtain the volume scooped; gravitational acceleration and solid properties complete the procedure and should give us the same value of ≈ 53.04 kN.

$$A = \int_{T_i}^{T_f} Pile(s) - Bkt(s) \, dt = 0.75 \; m^2 \quad \longrightarrow \quad V = A \, bkt_{width} = 2.025 \; m^3 \qquad (6.9)$$

thus:

$$F3 = V \, \vec{g} \, \rho \approx 53.04 kN \tag{6.10}$$

Hence, we can state the the payload computation reflects the expectations. Moving to the frictional force F4, as shown in Fig. 6.12, we obtain a sensed trend since we have an increasing amplitude reaching a maximum value at half simulation, when the payload starts being consistent and the force given by the virtual wall is at its maximum, as we will see shortly.
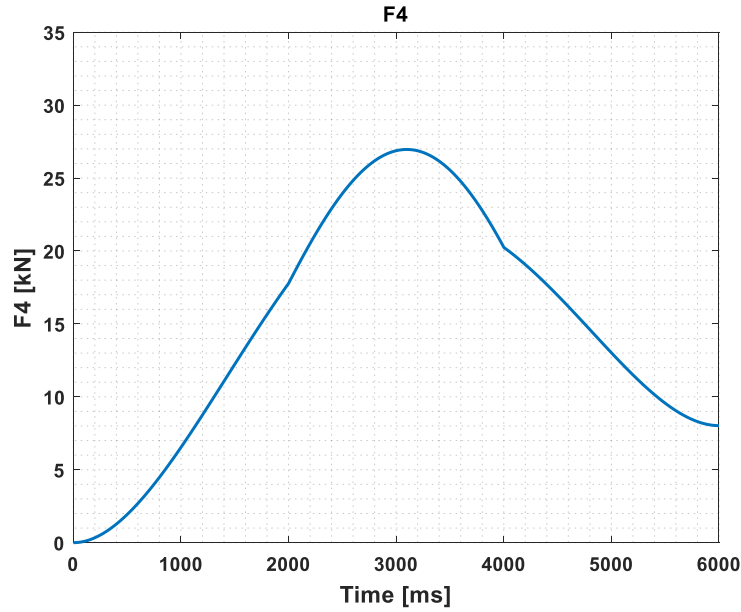

FIGURE 6.12: Frictional force F4 trend over time

The constant velocity during the whole operation leads to an always present $\dot{x}_{rel}$, that, recalling equation 6.5, implies the presence of frictional effects inside the bucket. If the bucket stopped, F4 would drop to zero since no relative velocity between materials and bucket would be present. As stated for the resistive force F1, also here we can also assume correct values and trend for frictional effects leaving a more concrete validation to the future works proposed in chapter 8.

Finally, the attention can be moved to the last an most important plot, shown in Fig. 6.6, expressing the force given by the soil pressure using Coulombs formulation.

As for F1, also F5 depends on the sinkage depth, but quadratically. Therefore, the overall trend that we are expecting is the one obtained, meaning that a climax is reached when H_{max} is obtained. The force required to move the material in front of the bucket increases with the machine entering into the pile; afterwards, also due to the tilting command that after three seconds from the simulation start reaches a considerable value of 30 °, the force required starts decreasing until a null value when the bucket exits the pile, as it was
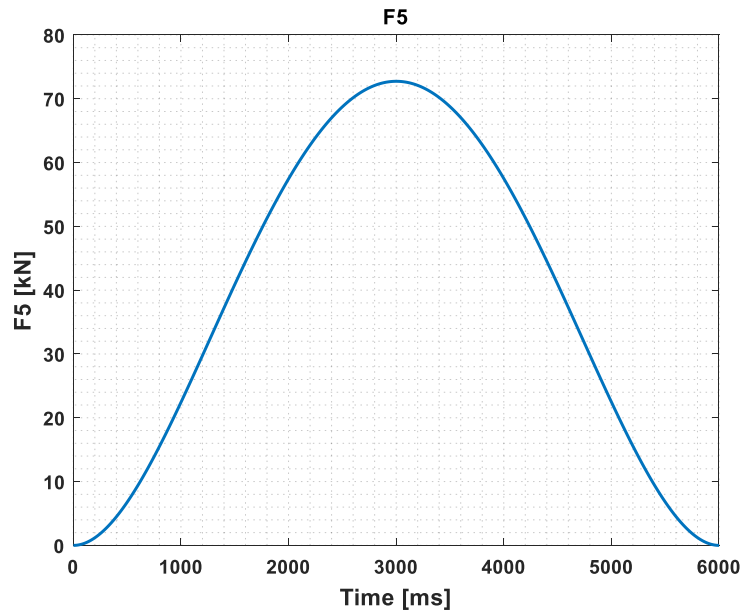
FIGURE 6.13: Force required to move the material in front of the bucket F5 trend over time

happening for the resistive force at the bucket tip F1.

It is important to state one more time that this simulated model has been developed in order to increase the performance of an overall traction control system. Due to the lack of available time, this new concept of pile model could not have been validated or verified neither via simulated software tools, nor via experimental data. Nevertheless, an solid part of the design has already been performed and the validation should not be too difficult, as it will be explained in a more complete way in the future work section. In conclusion, we can state that the overall behavior of the model is anyways acceptable, since at least the force trends reflects the expectations and moreover, the payload computation was validated throughout a few simple mathematical steps.

Chapter 7

Conclusions

This work outlines the activities involved in the development and experimental valida-
tion of an implement-chassis interaction model designed for heavy duty off-road vehicles.
Using a 16-tons wheel loader as a reference machine, the system was developed firstly
through the construction of an analytical simulation model. A basic vehicle dynamics
simulation model was developed too, accounting for all the forces exchanged between the
implement itself and the external world through the bucket during excavation cycles, and
the reaction forces acting on the implement hinges. This was further improved by the val-
idation brought through a developed simulated numerical model. By using MATLAB and
Simulink as software environments, a comparison between the analytical and numerical
simulated models have been performed bringing positive results. Thanks to this, the ac-
tual realization of the model for real-world system was possible. After some modifications
needed to bring the model into an available tool for the reference machine, a LABVIEW
code was developed in order to reflect the functionalities achieved in the MATLAB model.
In order to bring the model to real-time operation some modifications and tunings to the
reference machine were needed: the installation and calibration of pressure and angle
sensors. Once all the set-up was completed, a final experimental test validation was per-
formed in order to verify the results obtained for the simulated models. Acceptable and
solid comparison data was the final outcome of the experimental validations. The lifting
and tilting resulting forces matched in a smooth trend the simulated ones with clearly
some expected and explained differences. Nevertheless, a possible future work could inte-
grate some additional informations here neglected bringing the aforementioned differences
to be homogeneously negligible, as will be mentioned in the next chapter.

Moreover, as final work, an investigation to develop a new pile model with a multi-component digging force analysis was successfully performed. By starting from works found in literature, a Simulink model was developed and simulated. Clearly, since we are discussing on a simulated model, no experimental verification was possible. Nevertheless, a few validation aimed possibilities are left and discussed for research plan and future work in the following chapter.

Chapter 8

Future Work

This work represents the results obtained after an eight months window but it is intended to be expanded upon in the future by new students and researchers. To that end, this chapter outlines some work enhancements available for the developed model that are catalogued as worth to be completed in order to achieve a more complete and better performing operating system. Some of the limitations on the work done by the research team on the reference machine thus far have been imposed by the fact that it was funded by an industry sponsor, with their requirements dictating the focus of the research. Most of the work yet to be accomplished deals with expanding the scope beyond that set by the sponsor. Therefore, the nature of the future work is relatively theoretical and esoteric. These topics aim in improving the system overall behavior by expanding its complexity and taking into consideration features that had been neglected for simplification purposes:

1. **Include inertial and frictional effects on the static force analysis for the analytical simulated model** $\longrightarrow$ with the assumption of slow movements or constant velocities, during the development phase of our model, inertial terms have been neglected. Moreover, since the reference machine was a 16-tons wheel loader (discretely big vehicle), the assumption of small frictional forces with respect to the ones always in play during steady or scooping operations was done. These two assumptions were mainly made for accelerating the project development phase and were reasonable for the aforementioned reasons. Nevertheless, including these two terms in the analytical model equations should not require too much time and effort. Besides, especially by including inertial terms, the overall system behaviur would gain also correct dynamic measurements without performing them just in steady state operations. By doing so, it is also worth of mention that a possible experimental validation of the new concept of pile model explained in chapter 8 could be

achieved. Currently, since the system is developed just for steady state operations, this validation was not an option since, in order to validate the pile model, reaction forces exchanged during all the digging operation would be required. Therefore, it is clear now how by just including inertial terms into the system model, the power-fulness and usefulness of this would strongly increase.

2. **Include $\overline{FG}$ link and hydraulic actuators weights** $\longrightarrow$ assumptions of weight-less components were made during the project phase. In order again to simplify the system and decrease the development time required, some of the components with relatively low weight (all of them ≤ 100kg, that for a 16-tons machine could be easily considered low weight) were assumed just fixed rigid bodies transmitting the forces acting on them along their structure. Again, this was a good assumption that did not bring any unexpected or undesired relevant error (with respect to the numerical model, that was including them all). Nevertheless, with some extra time, including this resistive gravitational forces to the system would take too long and would surely increase the accuracy and precision of the overall system.

3. **Implement a test rig able to validate with accuracy the horizontal force estimate** $\longrightarrow$ regarding the vertical and horizontal external force estimate through the use of the inverse procedure explained and exploited in chapter 5.4, we saw how, throughout the utilization of a mine scale, a proper payload verification was possible and accurate achieving a percentage error with respect to a guaranteed reference. The horizontal force estimate was assumed to be correct within a reasonable range: if a wrong horizontal estimate was recorded, also a wrong payload would have prob-ably achieved. Nevertheless, having a proper test rig validating with accuracy the horizontal force too would be a nice feature. For example, renting or buying a pre-known very stiff spring and having the wheel loader pushing through it would be a reasonable verification with proper measured data comparable as it was done for the payload.

4. **Pile model validation through the use of EDEM software** $\longrightarrow$ EDEM is the market-leading Discrete Element Method (DEM) software for bulk material simulation. Used for tons of different simulation purposes, this powerful software is able to simulate excavation cycles for every off-road machinery. With the utilization of a co-simulation motion software, data is inter-exchanges between them: EDEM provides the forces exchanged during the scooping while the motion simulator gets those inputs in order to compute the respective motion properties as displacement, velocity and acceleration. Therefore, with a co-simulation through Simulink and EDEM, a validation of the pile model expressed in chapter 6 could be possible since the EDEM output exactly matches the force sought to be expressed by the

pile model. A final double-check can also be performed after the incorporation of inertial effects into the analytical model: pile model and EDEM software can be compared to data obtained through real-world digging cycles achieved by the use of the completed analytical model.

Bibliography

[1] Sarata Shigeru, Osumi Hisashi, Hirai Yusuke, and Matshushima Gen. Trajectory arrangement of bucket motion of wheel loader, 09 2003.

[2] Michael D. Worley and Valeria LaSaponara. Development of a simplified load-cycle model for wheel loader design, 01 2006.

[3] Yuta Takahashi, R. Yasuhara, Osamu Kanai, and Hisashi Osumi. Development of bucket scooping mechanism for analysis of reaction force against rock piles. 2006.

[4] Ahmad Hemami. Motion trajectory study in the scooping operation of an lhd-loader, 09 1994.

[5] Ahmad Hemami and L Daneshmend. Force analysis for automation of the loading operation in an l-h-d loader, 06 1992.

[6] M.G. Bekker. *Introduction to terrain-vehicle systems*. University of Michigan Press, 1969.

[7] E McKyes. *Soil Cutting and Tillage*. Oxford : Elsevier Science, 1985.

[8] A. Vacca D. Colombara, A. Alexander. Analysis of dynamics and force estimation for a wheel loader implement, 12 2018.

[9] Yongjie Lu Shaopu Yang and Shaohua Li. An overview on vehicle dynamics, 12 2013.

[10] T. D. Gillespie. Fundamentals of vehicle dynamics, 1992.

[11] Reza N. Jazar. Vehicle dynamics: Theory and application, 2014.

[12] Rajesh Rajamani. Vehicle dynamics and control, 2012.

[13] Aaron Shatters. Method and system for estimating payload weight with tilt position compensation, 10 2016.

[14] Wooyong Jung Hyunkoo Kang and Choon Lee. Modeling and measurement of payload mass of the wheel loader in the dynamic state based on experimental parameter identi cation., 05 2016.

[15] Matteo Corno Mara Tanelli and Sergio M. Savaresi. Modelling, simulation and control of two-wheeled vehicles, 02 2014.

[16] J. Y. Wong. Theory of ground vehicles, 2008.

[17] Viachaslau I. Kabanau Aleksandr Fedorovich Andreev and V. V. Vantsevich. Driveline systems of ground vehicles: Theory and design., 2010.

[18] Manfred Hiller Dieter Schramm and Roberto Bardini. Vehicle dynamics: Modeling and simulation., 2014.

[19] F. Montanaro G. Mastinu, S. Gaiazzi and D. Pirola. A semi-analytical tyre model for steady- and transient-state simulations., 01 1997.

[20] J. E. Bernard and C. L. Clover. Tire modeling for low-speed and high-speed calculations., 02 1995, Society of Automotive Engineers.